

To Reviewer #1:

We appreciate the reviewer for the positive comments. We have responded to all your comments and cited the references you recommended. Below are the reviewer's comments, followed by our responses and changes in manuscript.

Sincerely,

Shufen Pan (on behalf of the author team)

[Reviewer #1 General Comment] The authors provide a nice refresh reviewing global ET data products. Generally, it's a good literature review. Overall, however, the paper is excessively long and unfocused. Basically, the authors took a bunch of data products, calculated different comparative statistics, and discussed some patterns. That said, the title accurately depicts the unfocused nature of the paper, so it should not come as a surprise. The authors did try to throw in some science by looking at controls over ET, but this only served to make the paper even longer and more spread thin. Moreover, this type of product review has already been done by Mueller, Jimenez and others, so the novelty here is light. The science focus and strength are mostly on the land surface models, while the remote sensing is noticeably weak (there might be zero ET remote sensing authors on the list of 15 authors). The balanced title does not reflect the unbalanced paper. In general, I liked the paper as a source for a lit review.

[Response] We thank the reviewer for the positive comments. We admit that our paper is long. It is mainly because our study included a plenty of ET products of different types and we reviewed their principles, advantages, disadvantages and future directions. However, we think these descriptions and discussions are necessary because they give readers a comprehensive understanding in the strengths and limitations of each ET model and shows them possible solutions for overcoming the uncertainties identified in our analyses. As you stated, Mueller et al. (2011) and Jimenez et al. (2011) conducted analyses on different ET products. Nevertheless, the focus of our paper is different from theirs. Mueller et al. (2011) mainly focused on comparing IPCC AR4

ET estimates and observations-based ET estimates. Jimenez et al. (2011) mainly focused on the intercomparison of the seasonal variability of different latent heat, sensible heat and net radiative heat fluxes. Few discussion on the source of uncertainty and suggestions for future development was given. In comparison, our study emphasized on the analyses of uncertainty sources in different types of ET estimations and on the solutions for overcoming these identified uncertainties. In addition, our study incorporated ET estimates from fourteen state-of-the-art land surface models joining in the Trends and Drivers of the Regional Scale Sources and Sinks of Carbon Dioxide (TRENDY) Project, which is our strength over the previous studies. We want to clarify that although there is no ET remote sensing author on the list of 15 authors of our first version, the parts regarding remote sensing-based physical models have similar length with that of land surface models and machine learning algorithms in the text. As a synthesis of ET estimates from different approaches, we didn't focus too much on either land surface models or remote sensing-based models. In addition, Steven W Running, an expert in the area of remote sensing based ET, joined our author team and proposed several constructive suggestions which improved our manuscript. We proposed that terrestrial ET also has a potential planetary boundary (Page32 Line617-629 of the revised manuscript).

According to the references you recommended, we added citations and several sentences about the future development of remote sensing based ET models (Page35 Line671-679 of the revised manuscript).

“Most existing remote sensing-based ET studies focused on total ET, however, the partitioning of ET between transpiration, soil evaporation, and canopy interception may have significant divergence even though the total ET is accurately estimated (Talsma et al., 2018b). In current remote sensing-based ET models, soil evaporation, which is sensitive to precipitation events and soil moisture, is the part with the largest error (Talsma et al., 2018a). Therefore incorporating the increasing accessible satellite-based precipitation, soil moisture observations and soil property data will contribute to the improvement of soil evaporation estimation. Meanwhile, the consideration of soil evaporation under herbaceous vegetation and canopy will also reduce the errors.”

References

- Mueller, B., Seneviratne, S.I., Jimenez, C., Corti, T., Hirschi, M., Balsamo, G., Ciais, P., Dirmeyer, P., Fisher, J., Guo, Z. (2011) Evaluation of global observations - based evapotranspiration datasets and IPCC AR4 simulations. *Geophysical Research Letters* 38.
- Jimenez, C., Prigent, C., Mueller, B., Seneviratne, S.I., McCabe, M., Wood, E., Rossow, W., Balsamo, G., Betts, A., Dirmeyer, P. (2011) Global intercomparison of 12 land surface heat flux estimates. *Journal of Geophysical Research: Atmospheres* 116.
- Talsma, C., Good, S., Miralles, D., Fisher, J., Martens, B., Jimenez, C., Purdy, A. (2018a) Sensitivity of Evapotranspiration Components in Remote Sensing-Based Models. *Remote Sensing* 10, 1601.
- Talsma, C.J., Good, S.P., Jimenez, C., Martens, B., Fisher, J.B., Miralles, D.G., McCabe, M.F., Purdy, A.J. (2018b) Partitioning of evapotranspiration in remote sensing-based models. *Agricultural and Forest Meteorology* 260-261, 131-143.

To Reviewer #2:

We appreciate the reviewer for the positive comments. We have addressed the stated comments point-by-point. Below are the reviewer's comments, followed by our responses and changes in manuscript.

Sincerely,

Shufen Pan (on behalf of the author team)

[Reviewer #2 General Comment] This paper was already well-written, especially for the detailed discussion of limitations and possible next steps of different ET products. The reviewer thus has a few minor suggestions for the authors to consider.

[Response] We appreciate the reviewer for the positive comments.

[Reviewer #2 Specific Comment 1] The remote-sensing based, machine learning, and LSMs ET were comprehensively intercompared. However, how is the performance of ET outputs from the Earth system models (e.g., those from CMIP5 and CMIP6) and the reanalysis? There must be a reason why the authors did not include them. But please clarify this or add these comparison results.

[Response] Thanks for pointing out this issue. We didn't include ET outputs from the Earth system models (e.g., those from CMIP5 and CMIP6) because previous study confirmed systematic biases in global terrestrial ET estimated by CMIP5 models (Mueller and Seneviratne, 2014) and CMIP6 data were not available when we conducted our analyses. Reanalysis systems which are built upon the assimilation of extensive disparate observations in a physically consistent manner are capable of providing the estimates for a broad range of variables (Balsamo et al., 2015; Rienecker et al., 2011). ET estimates derived from both atmospheric and off-line land reanalysis datasets have been evaluated at local, regional and global scales (Baik et al., 2018; Feng et al., 2019; Mao and Wang,

2017) and have been compared with estimates from other approaches (Jimenez et al., 2011; Mueller et al., 2013; Mueller et al., 2011). The objective of this study is to identify the uncertainty sources in each type of ET estimations. However, these reanalysis systems integrate multiple process modules, multi-source remote sensing observations and ground-based measurements, and multiple assimilation algorithms, which lead to the accumulation of systematic errors and makes it hard to identify the sources of errors in ET estimations at the global scale. For above-mentioned reasons, our analyses didn't include ET outputs from the Earth system models and the reanalysis.

[Reviewer #2 Specific Comment 2] In lines 245-246, you indicated the benchmarking products are from the machine learning and physicalbased satellite datasets. It seems confusing both here and in Figs 3, 5, and 7. For example, in Fig. 7, if the benchmark product is the simple combination of the two data

[Response] The ensemble mean of benchmark products was calculated as the mean value of all machine learning and physical-based satellite estimates (6 datasets for Fig. 3 and 5, and 5 datasets for Fig. 7) rather than the mean value of machine learning ensemble mean and satellite ensemble mean, since we treated each benchmark dataset equally. We have added the sentence describing the calculation of the ensemble mean of benchmark products in section 2.2 (Page11 Line243-245).

“The ensemble mean of benchmark products was calculated as the mean value of all machine learning and physical-based satellite estimates since we treated each benchmark dataset equally.”

[Reviewer #2 Specific Comment 3] The Abstract seems quite long. Please double check if the Abstract length fits this particular journal.

[Response] We have double checked journal's requirements for manuscript, there is no particular limitation on the length of abstract. Following your comment, we have shortened the abstract.

“Evapotranspiration (ET) is critical in linking global water, carbon and energy cycles. Yet direct measurement of global terrestrial ET is not feasible. Here, we first summarized the basic theory and state-of-the-art approaches for estimating global terrestrial ET, including remote sensing-based physical models,

machine learning algorithms and land surface models (LSMs). We then utilized four remote sensing-based physical models, two machine-learning algorithms and fourteen LSMs to analyze the spatial and temporal variations in global terrestrial ET. The results showed that the ensemble means of annual global terrestrial ET estimated by these three categories of approaches agreed well, ranging from 589.6 mm yr⁻¹ to 617.1 mm yr⁻¹. For the period 1982-2011, both the ensembles of remote sensing-based physical models and machine-learning algorithms suggested positive trends in global terrestrial ET (0.62 mm yr⁻², $p < 0.05$ and 0.38 mm yr⁻², $p < 0.05$, respectively). In contrast, the ensemble mean of LSMs showed no statistically significant change (0.23 mm yr⁻², $p > 0.05$), even though many of the individual LSMs reproduced a positive trend. Nevertheless, all the twenty models used in this study showed anthropogenic earth greening had a positive role in increasing terrestrial ET. The concurrent small inter-annual variability, i.e. relative stability, found in all estimates of global terrestrial ET, suggests there exists a potential planetary boundary in regulating global terrestrial ET, with the value being about $6.74 \times 10^4 \text{ km}^3 \text{ yr}^{-1}$ (603 mm yr⁻¹). Uncertainties among approaches were identified in specific regions, particularly in the Amazon Basin and arid/semi-arid regions. Improvements in parameterizing water stress and canopy dynamics, utilization of new available satellite retrievals and deep learning methods, and model-data fusion will advance efforts in terrestrial ET estimates.”

[Reviewer #2 Specific Comment 4] In line 483, Fig. 5 does not have subfigures.

[Response] We are sorry for the wrong numbering. “Fig. 5c-d” in our previous manuscript should be “Fig. 8c-d”. We have corrected this error in the main text.

References

- Baik, J., Liaqat, U.W., Choi, M. (2018) Assessment of satellite- and reanalysis-based evapotranspiration products with two blending approaches over the complex landscapes and climates of Australia. *Agricultural and Forest Meteorology* 263, 388-398.
- Balsamo, G., Albergel, C., Beljaars, A., Boussetta, S., Brun, E., Cloke, H., Dee, D., Dutra, E., Muñoz-Sabater, J., Pappenberger, F. (2015) ERA-Interim/Land: a global land surface reanalysis data set. *Hydrology and Earth System Sciences* 19, 389-407.

Feng, T., Su, T., Zhi, R., Tu, G., Ji, F. (2019) Assessment of actual evapotranspiration variability over global land derived from seven reanalysis datasets. *International Journal of Climatology* 39, 2919-2932.

Jimenez, C., Prigent, C., Mueller, B., Seneviratne, S.I., McCabe, M., Wood, E., Rossow, W., Balsamo, G., Betts, A., Dirmeyer, P. (2011) Global intercomparison of 12 land surface heat flux estimates. *Journal of Geophysical Research: Atmospheres* 116.

Mao, Y., Wang, K. (2017) Comparison of evapotranspiration estimates based on the surface water balance, modified Penman - Monteith model, and reanalysis data sets for continental China. *Journal of Geophysical Research: Atmospheres* 122, 3228-3244.

Mueller, B., Hirschi, M., Jimenez, C., Ciais, P., Dirmeyer, P., Dolman, A., Fisher, J., Jung, M., Ludwig, F., Maignan, F. (2013) Benchmark products for land evapotranspiration: LandFlux-EVAL multi-data set synthesis. *Hydrology and Earth System Sciences*.

Mueller, B., Seneviratne, S.I. (2014) Systematic land climate and evapotranspiration biases in CMIP5 simulations. *Geophysical Research Letters* 41, 128-134.

Mueller, B., Seneviratne, S.I., Jimenez, C., Corti, T., Hirschi, M., Balsamo, G., Ciais, P., Dirmeyer, P., Fisher, J., Guo, Z. (2011) Evaluation of global observations - based evapotranspiration datasets and IPCC AR4 simulations. *Geophysical Research Letters* 38.

Rienecker, M.M., Suarez, M.J., Gelaro, R., Todling, R., Bacmeister, J., Liu, E., Bosilovich, M.G., Schubert, S.D., Takacs, L., Kim, G.-K., Bloom, S., Chen, J., Collins, D., Conaty, A., da Silva, A., Gu, W., Joiner, J., Koster, R.D., Lucchesi, R., Molod, A., Owens, T., Pawson, S., Pegion, P., Redder, C.R., Reichle, R., Robertson, F.R., Ruddick, A.G., Sienkiewicz, M., Woollen, J. (2011) MERRA: NASA's Modern-Era Retrospective Analysis for Research and Applications. *Journal of Climate* 24, 3624-3648.

List of relevant changes made in the manuscript

- (1) We shortened the abstract.
- (2) We added one section 4.1.6 which is focused on ET variability across precipitation gradient and the ET planetary boundary.
- (3) We added one paragraph in section 4.2.1 discussing the estimation of soil evaporation by remote sensing models.
- (4) We corrected a few grammatical mistakes.
- (5) We added two coauthors: Julia E.M.S. Nabel and Steven W. Running.

1 **Evaluation of global terrestrial evapotranspiration by state-of-the-art**
2 **approaches in remote sensing, machine learning, and land surface models**

3 Shufen Pan¹, Naiqing Pan^{1,2}, Hanqin Tian¹, Pierre Friedlingstein³, Stephen Sitch⁴, Hao Shi¹,
4 Vivek K. Arora⁵, Vanessa Haverd⁶, Atul K. Jain⁷, Etsushi Kato⁸, Sebastian Lienert⁹, Danica
5 Lombardozi¹⁰, Julia E.M.S. Nabel¹¹, Catherine ~~Ottle¹¹~~ Ottlé¹², Benjamin ~~Poulter¹²~~ Poulter^{13,14},
6 Sönke Zaehle¹⁴, Steven W. Running¹⁵

Formatted: Font: (Default) Times New Roman, 12 pt

Formatted: Superscript

7 ¹International Center for Climate and Global Change Research, School of Forestry and Wildlife
8 Sciences, Auburn University, Auburn, AL 36832, USA

9 ²State Key Laboratory of Urban and Regional Ecology, Research Center for Eco-Environmental
10 Sciences, Chinese Academy of Sciences, Beijing 100085, China

11 ³College of Engineering, Mathematics and Physical Sciences, University of Exeter, Exeter EX4
12 4QF, United Kingdom

13 ⁴College of Life and Environmental Sciences, University of Exeter, Exeter EX4 4RJ, United
14 Kingdom

15 ⁵Canadian Centre for Climate Modelling and Analysis, Environment Canada, University of
16 Victoria, Victoria, BC, Canada

17 ⁶CSIRO Oceans and Atmosphere, GPO Box 1700, Canberra, ACT 2601, Australia

18 ⁷Department of Atmospheric Sciences, University of Illinois, Urbana, IL 61801, USA

19 ⁸Institute of Applied Energy (IAE), Minato-ku, Tokyo 105-0003, Japan

20 ⁹Climate and Environmental Physics, Physics Institute, University of Bern, Bern, Switzerland

21 ¹⁰Climate and Global Dynamics Laboratory, National Center for Atmospheric Research,
22 Boulder, CO 80305, USA.

23 ¹¹Max Planck Institute for Meteorology, Bundesstr. 53, 20146 Hamburg, Germany

Formatted: Superscript

24 ¹¹~~LSCE~~¹²LSCE-IPSL-CNRS, Orme des Merisiers, 91191, Gif-sur-Yvette, France

25 ¹²~~NASA~~-¹³NASA Goddard Space Flight Center, Biospheric Science Laboratory, Greenbelt, MD
26 20771, USA

27 ¹³~~Department of Ecology, Montana State University, Bozeman, MT 59717, USA~~

28 ¹⁴Max Planck Institute for Biogeochemistry, P.O. Box 600164, Hans-Knöll-Str. 10, 07745 Jena,
29 Germany

30 ¹⁵Numerical Terradynamic Simulation Group, College of Forestry & Conservation, University of
31 Montana, Missoula, MT 59812, USA

Formatted: Font color: Auto

32
33 *Corresponding author: panshuf@auburn.edu, Tel: 1-334-844-1015

34 Abstract

35 Evapotranspiration (ET) is a critical component in linking global water cycle and links terrestrial
36 global water, carbon and energy cycles. ~~Accurate estimate of terrestrial ET is important for~~
37 ~~hydrological, meteorological, and agricultural research and applications, such as quantifying~~
38 ~~surface energy and water budgets, weather forecasting, and scheduling of irrigation. However, Yet~~
39 direct measurement of global terrestrial ET is not feasible. Here, we first ~~gave a retrospective~~
40 ~~introduction to~~summarized the basic theory and ~~recent developments of~~ state-of-the-art approaches
41 for estimating global terrestrial ET, including remote sensing-based physical models, machine
42 learning algorithms and land surface models (LSMs). ~~Then, w~~We then utilized ~~six remote sensing~~
43 ~~based models (including four remote sensing-based physical models and two machine-learning~~
44 ~~algorithms)~~ and fourteen LSMs to analyze the spatial and temporal variations in global terrestrial
45 ET. The results showed that the ensemble means of annual global terrestrial ET estimated by these
46 three categories of approaches agreed well, ranging from 589.6 mm yr⁻¹ to 617.1 mm yr⁻¹.~~the mean~~

47 ~~annual global terrestrial ET ranged from $50.7 \times 10^3 \text{ km}^3 \text{ yr}^{-1}$ (454 mm yr^{-1}) to $75.7 \times 10^3 \text{ km}^3 \text{ yr}^{-1}$~~
48 ~~(697 mm yr^{-1}) , with the average being $65.5 \times 10^3 \text{ km}^3 \text{ yr}^{-1}$ (588 mm yr^{-1}), during 1982-2011. LSMs~~
49 ~~had significant uncertainty in the ET magnitude in of tropical regions, especially the Amazon~~
50 ~~Basin, while remote sensing-based ET products showed larger inter-model range in arid and semi-~~
51 ~~arid regions than LSMs. LSMs and remote sensing-based physical models presented much larger~~
52 ~~inter-annual variability (IAV) of ET than machine learning algorithms in southwestern U.S. and~~
53 ~~the Southern Hemisphere, particularly in Australia. LSMs suggested stronger control of~~
54 ~~precipitation on ET IAV than remote sensing-based models. For the period 1982-2011, both The~~
55 ~~the ensembles of remote sensing-based physical models and machine-learning algorithms~~
56 ~~suggested significant increasing positive trends in global terrestrial ET (at the rate of 0.62 mm yr^{-2}~~
57 ~~$(p < 0.05)$ and 0.38 mm yr^{-2} , ($p < 0.05$), respectively). In contrast, the ensemble mean of LSMs~~
58 ~~showed no statistically significant change (0.23 mm yr^{-2} , $p > 0.05$), even though most many of the~~
59 ~~individual LSMs reproduced the a increasing positive trend. Nevertheless, all the twenty models~~
60 ~~used in this study showed anthropogenic earth greening had a positive role in increasing terrestrial~~
61 ~~ET. The concurrent small inter-annual variability, i.e. relative stability, found in all estimates of~~
62 ~~global terrestrial ET, suggests there exists a potential planetary boundary in regulating global~~
63 ~~terrestrial ET, with the value being about $6.74 \times 10^4 \text{ km}^3 \text{ yr}^{-1}$ (603 mm yr^{-1}). Moreover, all models~~
64 ~~suggested a positive effect of vegetation greening on ET intensification. Spatially, all methods~~
65 ~~showed that ET significantly increased in western and southern Africa, western India and~~
66 ~~northeastern Australia, but decreased severely in southwestern U.S., southern South America and~~
67 ~~Mongolia. Discrepancies in ET trend mainly appeared in tropical regions like the Amazon Basin.~~
68 ~~The ensemble means of the three ET categories showed generally good consistency, however,~~
69 ~~considerable uncertainties among approaches were identified in specific regions, particularly in~~

70 ~~the Amazon Basin and arid/semi-arid regions, still exist in both the temporal and spatial variations~~
71 ~~in global ET estimates. The uncertainties were induced by multiple factors, including~~
72 ~~parameterization of land processes, meteorological forcing, lack of in situ measurements, remote~~
73 ~~sensing acquisition and scaling effects. Improvements in the representation of parameterizing water~~
74 ~~stress and canopy dynamics, are essentially needed to reduce uncertainty in LSM simulated ET.~~
75 ~~Utilization utilization of latest new available satellite sensors retrievals and deep learning methods,~~
76 ~~theoretical advancements in nonequilibrium thermodynamics, and application of integrated~~
77 ~~methods that fuse different ET estimates or relevant key biophysical variables will improve the~~
78 ~~accuracy of remote sensing based physical models and model-data fusion will advance efforts in~~
79 ~~terrestrial ET estimates,~~

Formatted: Font: (Asian) SimSun

80

81

82

Formatted: Justified, Space After: 10 pt, Don't add space between paragraphs of the same style, Line spacing: Double, Don't suppress line numbers

83 **Keywords:** Evapotranspiration; Land surface models; Remote sensing; Machine learning.

84

85

86

87 **1. Introduction**

88 Terrestrial evapotranspiration (ET) is the sum of the water loss to the atmosphere from plant tissues
89 via transpiration and that from the land surface elements including soil, plants and open water
90 bodies through evaporation. Processes controlling ET play a central role in linking the energy
91 (latent heat), water (moisture flux), and carbon cycles (photosynthesis-transpiration trade-off) in
92 the earth system, of the atmosphere, hydrosphere and biosphere. Over 60% of precipitation on the
93 land surface is returned to the atmosphere through ET (Oki and Kanae, 2006), and the
94 accompanying latent heat (λET , λ is the latent heat of vaporization) accounts for more than half of
95 the solar energy received by the land surface (Trenberth et al., 2009). ET is also coupled with the
96 carbon dioxide exchange between canopy and atmosphere through vegetation photosynthesis.
97 These linkages make ET an important variable in both the short-term numerical weather
98 prediction and long-term climate simulations. Moreover, ET is an critical ~~excellent~~ indicator for
99 ecosystem functionings across a variety of spatial scales. For enhancing our predictive
100 understanding of earth system and sustainability, therefore, it is essential to a Accurately assess
101 estimation of land surface ET in a changing global environment and understanding of the
102 underlying mechanisms that affect ET variability are therefore essentially required to address a
103 series of climatic, hydrological, ecological and economic issues such as global warming, runoff
104 yield, droughts, and agricultural production.
105 However, ~~there still exists~~ large uncertainty still exists in quantifying the magnitude of global
106 terrestrial ET and its spatial and temporal patterns, despite extensive research (Allen et al., 1998;
107 Liu et al., 2008; Miralles et al., 2016; Mueller et al., 2011; Tian et al., 2010). The previous
108 estimates of global land mean annual ET range from 417 mm year^{-1} to 650 mm year^{-1} for the whole
109 or part of the 1982-2011 period (Mu et al., 2007; Mueller et al., 2011; Vinukollu et al., 2011a;

110 Zhang et al., 2010). This large discrepancy among independent studies may be attributed to lack
111 of sufficient measurements, uncertainty in forcing data, inconsistent spatial and temporal
112 resolutions, ill-calibrated model parameters and deficiencies in model structures. Of the four
113 components of ET (transpiration, soil evaporation, canopy interception, and open-water
114 evaporation), transpiration (T_v) contributes the largest uncertainty, as it is modulated not only by
115 surface meteorological conditions and soil moisture but also by the physiology and structures of
116 plants. Changes in non-climatic factors such as elevated atmospheric CO₂, nitrogen deposition,
117 and land covers also serve as influential drivers of T_v (Gedney et al., 2006; Mao et al., 2015; Pan
118 et al., 2018b; Piao et al., 2010). As such, the global ratio of transpiration to ET (T_v/ET) has long
119 been of debate, with the most recent observation-based estimate being 0.64 ± 0.13 constrained by
120 the global water-isotope budget (Good et al., 2015). Most earth system models are thought to
121 largely underestimate T_v/ET (Lian et al., 2018).

122 Global warming is expected to accelerate the hydrological cycle (Pan et al., 2015). For the period,
123 1982 to the late 1990s, ET was reported to increase by about 7 mm (~1.2%) per decade driven by
124 rising an increase in radiative forcing and consequently global and regional temperatures (Douville
125 et al., 2013; Jung et al., 2010; Wang et al., 2010). The contemporary near-surface specific humidity
126 also increased over both land and ocean (Dai, 2006; Simmons et al., 2010; Willett et al., 2007).
127 More recent studies confirmed that, since the 1980s, global ET has showeds an overall increase
128 (Mao et al., 2015; Yao et al., 2016; Zeng et al., 2018a; Zeng et al., 2012; Zeng et al., 2016; Zhang
129 et al., 2015; Zhang et al., 2016b). However, the magnitude and spatial distribution of such a trend
130 are far from determined. Over the past 50 years, pan evaporation decreased throughout the world
131 (Fu et al., 2009; Peterson et al., 1995; Roderick and Farquhar, 2002), implying an declining
132 tendency ofincrease in actual ET given the pan evaporation paradox. Moreover, the increase in

133 global terrestrial ET was found to cease or even be ~~even~~ reversed during 1998 to 2008, primarily
134 due to the decreased soil moisture supply in the Southern Hemisphere (Jung et al., 2010). To
135 reconcile the disparity, Douville et al. (2013) argued that the peak ET in 1998 should not be taken
136 as a tipping point because ET was estimated to increase in the multi-decadal evolution. More
137 efforts are needed to understand the spatial and temporal variations of global terrestrial ET and the
138 underlying mechanisms that control its magnitude and variability.

139 Conventional techniques, such as lysimeter, eddy covariance, large aperture scintillometer and the
140 Bowen ratio method, are capable of providing ET measurements at point and local scales (Wang
141 and Dickinson, 2012). However, it is ~~diffieult~~ impossible to directly measure ET at the global scale
142 because dense global coverage by such instruments is not feasible and the representativeness of
143 point-scale measurements to comprehensively represent the spatial heterogeneity of global land
144 surface is also doubtful (Mueller et al., 2011). To address this issue, numerous approaches have
145 been proposed in recent years to estimate global terrestrial ET and these approaches can be divided
146 into three main categories: 1) remote sensing-based physical models, 2) machine learning methods,
147 and 3) land surface models (Miralles et al., 2011; Mueller et al., 2011; Wang and Dickinson, 2012).

148 Knowledge of the uncertainties in global terrestrial ET estimates from different approaches is the
149 prerequisite for future projection and many other applications. In recent years, several studies have
150 compared multiple terrestrial ET estimates (Khan et al., 2018; Mueller et al., 2013; Wartenburger
151 et al., 2018; Zhang et al., 2016b). However, most of these studies ~~just~~ analyzed multiple datasets
152 of the same approach or focused on investigating similarities and differences among different
153 approaches. Few studies have been conducted to identify uncertainties in multiple estimates of
154 different approaches.

155 In this study, we integrate state-of-the-art estimates of global terrestrial ET, including data-driven
156 and process-based estimates, to assess its spatial pattern, inter-annual variability, environmental
157 drivers, long-term trend, and ~~reaction-response~~ to vegetation greening. Our goal is not to compare
158 the various models and choose the best one, but to identify the uncertainty sources in each type of
159 estimate and provide suggestions for future model development. In the following sections, we first
160 have a brief introduction to all methodological approaches and ET datasets used in this study.
161 ~~Second, we~~We then quantify the spatiotemporal variations in global terrestrial ET during the
162 period 1982-2011 by analyzing the results from the current state-of-the-art models. Finally, we
163 discuss ~~the required~~some suggested solutions for ~~overcoming~~reducing the ~~uncertainties~~
164 ~~identified~~identified uncertainties.

165 **2. Methodology and data sources**

166 **2.1 Overview of approaches to global ET estimation**

167 **2.1.1 Remote sensing-based physical models**

168 Satellite remote sensing has been widely recognized as a promising tool to estimate global ET,
169 because it is capable of providing spatially and temporally continuous measurements of critical
170 biophysical parameters affecting ET, including vegetation states, albedo, fraction of absorbed
171 photosynthetically active radiation, land surface temperature and plant functional types (Li et al.,
172 2009). Since the 1980s, a large number of methods have been developed using a variety of satellite
173 observations (Zhang et al., 2016a). However, part of these methods such as surface energy balance
174 (SEB) models and surface temperature-vegetation index (T_s -VI) ~~space methods~~ are usually applied
175 at local and regional scales. At the global scales, the vast majority of existing remote sensing-based
176 physical models can be categorized into two groups: the Penman-Monteith (PM) based and the
177 Priestley-Taylor (PT) based models.

178 A) Remote sensing models based on Penman-Monteith equation

179 The Penman equation, derived from the Monin-Obukhov similarity theory and surface energy
180 balance, uses surface net radiation, temperature, humidity, wind speed and ground heat flux to
181 estimate ET from an open water surface. For vegetated surfaces, canopy resistance was introduced
182 into the Penman equation by Monteith (Monteith, 1965) and the PM equation is formulated as:

$$183 \quad \lambda ET = \frac{\Delta(R_n - G) + \rho_a C_p VPD / r_a}{\Delta + \gamma(1 + r_s / r_a)} \quad (1)$$

184 where Δ , R_n , G , ρ_a , C_p , γ , r_s , r_a , VPD are the slope of the curve relating saturated water vapor
185 pressure to air temperature, net radiation, soil heat flux, air density, the specific heat of air,
186 psychrometric constant, surface resistance, aerodynamic resistance and vapor pressure deficit,
187 respectively. The canopy resistance term in the PM equation exerts a strong control on
188 transpiration. For example, based on the algorithm proposed by Cleugh et al. (2007), the MODIS
189 (Moderate Resolution Imaging Spectroradiometer) ET algorithm improved the model performance
190 through inclusion of environmental stress into canopy conductance calculation and explicitly
191 accounted for soil evaporation (Mu et al., 2007). Further, Mu et al. (2011) improved the MODIS
192 ET algorithm by considering nighttime ET, adding soil heat flux calculation, separating dry canopy
193 surface from the wet, and dividing soil surface into saturated wet surface and moist surface.
194 Similarly, Zhang et al. (2010) developed a Jarvis-Stewart-type canopy conductance model based
195 on normalized difference vegetation index (NDVI) to take advantage of the long-term Advanced
196 Very High Resolution Radiometer (AVHRR) dataset. More recently, this model was improved by
197 adding a CO₂ constraint function in the canopy conductance estimate (Zhang et al., 2015). Another
198 important revision for the PM approach is proposed by Leuning et al. (2008). The Penman-
199 Monteith-Leuning method adopts a simple biophysical model for canopy conductance, which can
200 account for influences of radiation and atmospheric humidity deficit. Additionally, it introduces a

201 simpler soil evaporation algorithm than that proposed by Mu et al. (2007), which potentially makes
202 it attractive to use with remote sensing. However, PM-based models have one intrinsic weakness:
203 temporal upscaling which is required in translating instantaneous ET estimation into a longer time-
204 scale value (Li et al., 2009). This could be easily done at the daily scale under clear-sky conditions
205 but faces challenge at weekly to monthly time-scales due to lack of ~~the~~ cloud coverage information.

206 B) Remote sensing models based on Priestley-Taylor equation

207 The Priestley-Taylor (PT) equation is a simplification of the PM equation without parameterizing
208 aerodynamic and surface conductances (Priestley and Taylor, 1972) and can be expressed as:

$$209 \quad \lambda ET = f_{stress} \times \alpha \times \frac{\Delta}{\Delta + \gamma} \times (R_n - G) \quad (2)$$

210 where f_{stress} is a stress factor and is usually computed as a function of environmental conditions. α
211 is the PT parameter with a value of 1.2–1.3 under water unstressed conditions and can be estimated
212 using remote sensing. Although the original PT equation works well in estimating potential ET
213 across most surfaces, the Priestley-Taylor coefficient, α , usually needs adjustment to convert
214 potential ET to actual ET (Zhang et al., 2016a). Instead, Fisher et al. (2008) developed a modified
215 PT model that keeps α constant but scales down potential ET by ecophysiological constraints and
216 soil evaporation partitioning. The accuracy of their model has been validated against eddy
217 covariance measurements conducted at a wide range of climates and plant functional types (Fisher
218 et al., 2009; Vinukollu et al., 2011b). Following this idea, Yao et al. (2013) further developed a
219 modified Priestley-Taylor algorithm that constrains soil evaporation using the Apparent Thermal
220 Inertia derived index of soil water deficit. Miralles et al. (2011) also proposed a novel PT type
221 model, Global Land surface Evaporation: the Amsterdam Methodology (GLEAM). GLEAM
222 combines a soil water module, a canopy interception model and a stress module within the PT
223 equation. The key distinguishing features of this model are the use of microwave-derived soil

224 moisture, land surface temperature and vegetation density, and the detailed estimation of rainfall
225 interception loss. In this way, GLEAM minimizes the dependence on static variables, avoids the
226 need for parameter tuning, and enables the quality of the evaporation estimates to rely on the
227 accuracy of the satellite inputs (Miralles et al., 2011). Compared with the PM approach, the PT
228 based approaches avoid the computational complexities of aerodynamic resistance and the
229 accompanying error propagation. However, the many simplifications and semi-empirical
230 parameterization of physical processes in the PT based approaches may lower its accuracy.

231 **2.1.2 ~~VI~~Vegetation index-based empirical algorithms and machine learning methods**

232 The principle of empirical ET algorithms is to link observed ET to its controlling environmental
233 factors through various statistical regressions or machine learning algorithms of different
234 complexities. The earliest empirical regression method was proposed by Jackson et al. (1977). At
235 present, the majority of regression models are based on vegetation indices (Glenn et al., 2010),
236 such as NDVI and enhanced vegetation index (EVI), because of their simplicity, resilience in the
237 presence of data gaps, utility under a wide range of conditions and connection with vegetation
238 transpiration capacity (Maselli et al., 2014; Nagler et al., 2005; Yuan et al., 2010). As an alternative
239 to statistical regression methods, machine learning algorithms have been gaining increased
240 attention for ET estimation ~~for~~ due to their ability to capture the complex nonlinear relationships
241 between ET and its controlling factors (Dou and Yang, 2018). Many conventional machine
242 learning algorithms, such as artificial neural networks, random forest, and support vector machine
243 based algorithms have been applied in various ecosystems (Antonopoulos et al., 2016; Chen et al.,
244 2014; Feng et al., 2017; Shrestha and Shukla, 2015) and have proved to be more accurate in
245 estimating ET than simple regression models (Antonopoulos et al., 2016; Chen et al., 2014; Kisi
246 et al., 2015; Shrestha and Shukla, 2015; Tabari et al., 2013). In up-scaling FLUXNET ET to the

247 global scale, Jung et al. (2010) used the model tree ensemble method to integrate eddy covariance
248 measurements of ET with satellite remote sensing and surface meteorological data. In a ~~latest~~
249 ~~recent~~ study (Bodesheim et al., 2018), the random forest approach was used to derive global ET at
250 a half-hourly time-scale.

251 **2.1.3 Process-based land surface models (LSMs)**

252 Although satellite-derived ET products have provided quantitative investigations of historical
253 terrestrial ET dynamics, they can only cover a limited temporal record of about four decades. To
254 obtain terrestrial ET before 1980s and predict future ET dynamics, LSMs are needed, as they are
255 able to represent a large number of interactions and feedbacks between physical, biological, and
256 biogeochemical processes in a prognostic way (Jimenez et al., 2011). ET simulation in LSMs is
257 regulated by multiple biophysical and physiological properties or processes, including but not
258 limited to stomatal conductance, leaf area, root water uptake, soil water, runoff and sometimes
259 nutrient uptake (Famiglietti and Wood, 1991; Huang et al., 2016; Lawrence et al., 2007). Although
260 almost all current LSMs have these components, different parameterization schemes result in
261 substantial differences in ET estimation (Wartenburger et al., 2018). Therefore, in recent years,
262 the multi-model ensemble approach has become popular in quantifying magnitude, spatiotemporal
263 pattern and uncertainty of ~~improving the accuracy of~~ global terrestrial ET ~~estimation~~ (Mueller et
264 al., 2011; Wartenburger et al., 2018). Yao et al. (2017) showed that a simple model averaging
265 method or a Bayesian model averaging method is superior to each individual model in predicting
266 terrestrial ET.

267 **2.2 Description of ET ~~datasets~~ models used in this study**

268 In this study, we evaluate twenty ET products that are based on remote sensing-based physical
269 models, machine-learning algorithms, and LSMs to investigate the magnitudes and spatial patterns

270 of global terrestrial ET over recent decades. Table 1 lists the input data, adopted ET algorithms,
271 limitations, and references for each product. We use a simple model averaging method when
272 calculating the mean value of multiple models.

273 Four physically-based remote sensing datasets, including Process-based Land Surface
274 Evapotranspiration/Heat Fluxes algorithm (P-LSH), Global Land surface Evaporation: the
275 Amsterdam Methodology (GLEAM), Moderate Resolution Imaging Spectroradiometer (MODIS)
276 and PML-CSIRO (Penman-Monteith-Leuning), and two machine-learning datasets, including
277 Random Forest (RF) and Model Tree Ensemble (MTE), are used in our study. Both machine
278 learning and physical-based remote sensing datasets (totally six datasets) were considered as
279 benchmark products. The ensemble mean of benchmark products was calculated as the mean value
280 of all machine learning and physical-based satellite estimates; since we treated each benchmark
281 dataset equally.

282 ~~P-LSH, MODIS and PML-CSIRO~~ Three of the four remote sensing-based ~~physically-based~~ models
283 quantify ET through PM approaches. P-LSH adopts a modified PM approach coupling with biome-
284 specific canopy conductance determined from NDVI (Zhang et al., 2010). The modified P-LSH
285 model used in this study also accounts for the influences of atmospheric CO₂ concentrations and
286 wind speed on canopy stomatal conductance and aerodynamic conductance (Zhang et al., 2015).
287 MODIS ET model is based on the algorithm proposed by Cleugh et al. (2007). Mu et al. (2007)
288 improved the model performance through the inclusion of environmental stress into canopy
289 conductance calculation, and explicitly accounting for soil evaporation by combing
290 complementary relationship hypothesis with PM equation. The MODIS ET product (MOD16A3)
291 used in this study was further improved by considering night-time ET, simplifying vegetation
292 cover fraction calculation, adding soil heat flux item, dividing saturated wet and moist soil,

Formatted: Automatically adjust right indent when grid is defined, Space After: 0 pt, Adjust space between Latin and Asian text, Adjust space between Asian text and numbers

Formatted: Font color: Auto

Formatted: Font color: Red

293 separating dry and wet canopy, as well as modifying algorithms of aerodynamic resistance,
294 stomatal conductance, and boundary layer resistance (Mu et al., 2011). PML-CSIRO adopts the
295 Penman-Monteith-Leuning algorithm, which calculates surface conductance and canopy
296 conductance by a biophysical model instead of classic empirical models. The maximum stomatal
297 conductance is estimated using the trial-and-error method (Zhang et al., 2016b). Furthermore, for
298 each grid covered by natural vegetation, the PML-CSIRO model constrains ET at the annual scale
299 using the Budyko hydrometeorological model proposed by Fu (1981). GLEAM ET calculation is
300 based on the PT equation, which requires less-fewer model inputs than PM equation, and the
301 majority of these inputs can be directly achieved from satellite observations. Its rationale is to
302 make the most of information about evaporation contained in the satellite-based environmental
303 and climatic observations (Martens et al., 2017; Miralles et al., 2011). Key variables including air
304 temperature, land surface temperature, precipitation, soil moisture, vegetation optical depth and
305 snow-water equivalent are satellite-observed. Moreover, the extensive usage of microwave remote
306 sensing products in GLEAM ensures the accurate estimation of ET under diverse weather
307 conditions. Here, we use the GLEAM v3.2 version which has overall better quality than previous
308 version (Martens et al., 2017).

309 The first used machine learning model, MTE, ~~approach~~ is based on the Tree Induction Algorithm
310 (TRIAL) and Evolving Trees with Random Growth (ERROR) algorithm (Jung et al., 2009). The
311 TRIAL grows model trees from the root node and splits at each node with the criterion of
312 minimizing the sum of squared errors of multiple regressions in both subdomains. ERROR is used
313 to select the model trees that are independent from each other and have best performances under
314 Schwarz criterion. Canopy fraction of absorbed photosynthetic active radiation (fAPAR),
315 temperatures, precipitation, relative humidity, sunshine hours, and potential radiation are used as

316 explanatory variables to train MTE (Jung et al., 2011). The second machine learning model is the
317 ~~rationale of~~ random forest (RF) algorithm whose rationale is generating a set of independent
318 regression trees through randomly selecting training samples automatically (Breiman, 2001). Each
319 regression tree is constructed using samples selected by bootstrap sampling method. After fixing
320 individual tree in entity, the final result is determined by simple averaging. One merit of RF
321 algorithm is its capability of handling complicated nonlinear problems and high dimensional data
322 (Xu et al., 2018). For the RF product used in this study, multiple explanatory variables including
323 enhanced vegetation index, fAPAR, leaf area index, daytime and nighttime land surface
324 temperature, incoming radiation, top of atmosphere potential radiation, index of water availability
325 and relative humidity were used to train regression trees (Bodesheim et al., 2018).

326 The fourteen LSMs-derived ET products were from the Trends and Drivers of the Regional Scale
327 Sources and Sinks of Carbon Dioxide (TRENDY) Project (including CABLE, CLASS-CTEM,
328 CLM45, DLEM, ISAM, JSBACH, JULES, LPJ-GUESS, LPJ-wsl, LPX-Bern, O-CN,
329 ORCHIDEE, ORCHIDEE-MICT and VISIT). Daily gridded meteorological reanalyses from the
330 CRU-NCEPv8 dataset (temperature, precipitation, long- and short-wave incoming radiation, wind-
331 speed, humidity, air pressure) were used to drive the LSMs. The TRENDY simulations were
332 performed in year 2017 and contributed to the Global Carbon Budget reported in Le Quéré et al.
333 (2018). We used the results of S3 experiment of TRENDYv6 (with changing CO₂, climate and
334 land use) over the period ~~1860-2016~~1982-2011, a time period consistent with other products
335 derived from remote sensing-based physical models and machine-learning algorithms.

336 **2.3 Description of other datasets**

337 To quantify the contributions of vegetation greening to terrestrial ET variations, we used the LAI
338 of TRENDYv6 S3 experiment. We also used the newest version of the Global Inventory Modeling
339 and Mapping Studies LAI data (GIMMS LAI3gV1) as satellite-derived LAI. GIMMS LAI3gV1
340 was generated from AVHRR GIMMS NDVI3g using an Artificial Neural Network (ANN) derived
341 model (Zhu et al., 2013). It covers the period 1982 to 2016 with bimonthly frequency and has a
342 $1/12^\circ$ spatial resolution. To achieve a uniform resolution, all data were resampled to $1/2^\circ$ using the
343 nearest neighbour method. ~~According to~~Following Pan et al. (2018a), grids with an annual mean
344 NDVI<0.1 were ~~thought-assumed~~ to be non-vegetated regions and were therefore masked out.
345 NDVI data ~~were~~are from GIMMS NDVI3gV1 dataset. Temperature, precipitation and radiation
346 are from CRU-NCEPv8.

347 **2.4 Statistical analysis**

348 The significance of ET trends is analyzed using the Mann-Kendall (MK) test (Kendall, 1955;
349 Mann, 1945). It is a rank-based non-parametric method that has been widely applied for detecting
350 a trend in hydro-climatic time series (Sayemuzzaman and Jha, 2014; Yue et al., 2002). The Theil-
351 Sen estimator was applied to estimate the magnitude of the slope. The advantage of this method
352 over ordinary least squares estimator is that it limits the influence of the outliers on the slope (Sen,
353 1968).

354 Terrestrial ET IAV is mainly controlled by variations in temperature, precipitation, and shortwave
355 solar radiation (Zeng et al., 2018b; Zhang et al., 2015). In this study, we performed partial
356 correlation analyses between ET and these three climatic variables at an annual scale for each grid
357 cell to explore climatic controls on ET IAV. Variability caused by climatic variables was assessed
358 through the square of partial correlation coefficients between ET and temperature, precipitation,
359 and radiation. We chose partial correlation analysis because it can quantify the linkage between

360 ET and a single environmental driving factor while controlling the effects of other remaining
 361 environmental factors. Partial correlation analysis is a widely applied statistical tool to isolate the
 362 relationship between two variables from the confounding effects of many correlated variables
 363 (Anav et al., 2015; Jung et al., 2017; Peng et al., 2013). All variables were first detrended in the
 364 statistical correlation analysis since we focus on the inter-annual relationship. The study period is
 365 from 1982 to 2011 for all models except MODIS and Rand Forest whose temporal coverage is
 366 limited to 2001-2011 because of data availability.

367 To quantify the contribution of vegetation greening to terrestrial ET, we separated the trend in
 368 terrestrial ET into four components induced by climatic variables and vegetation dynamics by
 369 establishing a multiple linear regression model between global ET and temperature, precipitation,
 370 shortwave radiation, and LAI (Eq. 3-4):

$$371 \quad \delta(ET) = \frac{\partial(ET)}{\partial(LAI)} \delta(LAI) + \frac{\partial(ET)}{\partial(T)} \delta(T) + \frac{\partial(ET)}{\partial(P)} \delta(P) + \frac{\partial(ET)}{\partial(R)} \delta(R) + \varepsilon \quad (3)$$

$$372 \quad \delta(ET) = \gamma_{ET}^{LAI} \delta LAI + \gamma_{ET}^T \delta T + \gamma_{ET}^P \delta P + \gamma_{ET}^R \delta R + \varepsilon \quad (4)$$

373 γ_{ET}^{LAI} , γ_{ET}^T , γ_{ET}^P , γ_{ET}^R are the sensitivities of ET to leaf area index (LAI), air temperature (T),
 374 precipitation (P), and radiation (R), respectively. ε is the residual, representing the impacts of other
 375 factors.

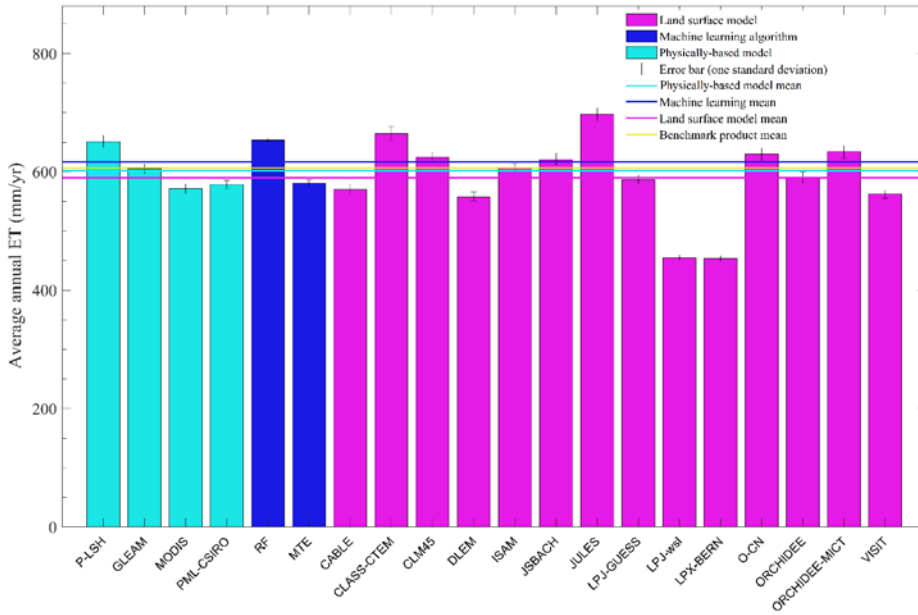
376 After calculating γ_{ET}^{LAI} , γ_{ET}^T , γ_{ET}^P , γ_{ET}^R , the contribution of trend in factor i ($Trend(i)$) ~~for~~ to the
 377 trend in ET ($Trend(ET)$) can be quantified as follows:

$$378 \quad Contri(i) = (\gamma_{ET}^i \times Trend(i)) / Trend(ET) \quad (5)$$

379 In performing multiple linear regression, we used GIMMS LAI for both remote sensing-based
 380 physical models and machine learning methods, and ~~used~~ individual TRENDYv6 LAI for each
 381 TRENDY model. The gridded data of Temperature, precipitation and radiation are from CRU-
 382 NCEPv8

383 **3. Results**

384 **3.1 The ET magnitude estimated by multiple models**



385

386 **Figure 1.** Average annual global terrestrial ET estimated by each model during the period 2001-
387 2011. Error bars represent the standard deviation of each dataset/model. The four lines indicate the
388 mean value of each category.

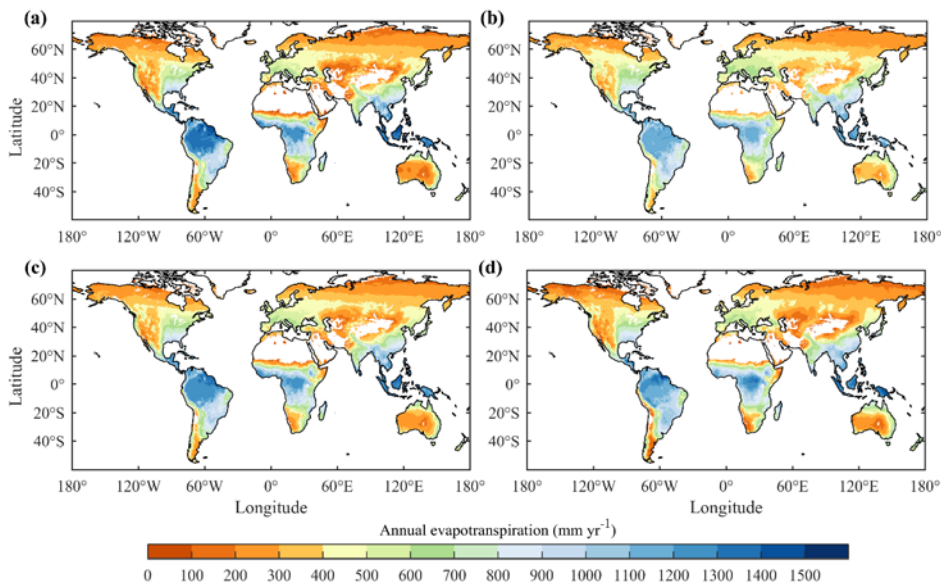
389 The multi-year ensemble mean of annual global terrestrial ET during 2001-2011 derived by the
390 machine learning methods, remote sensing-based physical models-methods and TRENDY models
391 agreed well, ranging from 589.6 mm yr⁻¹ to 617.1 mm yr⁻¹. However, substantial differences
392 existed among individual datasets-models (Fig. 1). LPJ-wsl (455.3 mm yr⁻¹) and LPX-Bern (453.7
393 mm yr⁻¹) estimated significantly lower ET than other models, even in comparison with most
394 previous studies focusing on earlier periods (Table S1). In contrary, JULES gave the largest ET

395 estimate (697.3 mm yr^{-1} , equals to $7.57 \times 10^4 \text{ km}^3 \text{ yr}^{-1}$) among ~~all models used in this study~~, and
396 showed an obvious increase of ET compared to its estimation during 1950-2000 ($6.5 \times 10^4 \text{ km}^3 \text{ yr}^{-1}$,
397 Table S1).

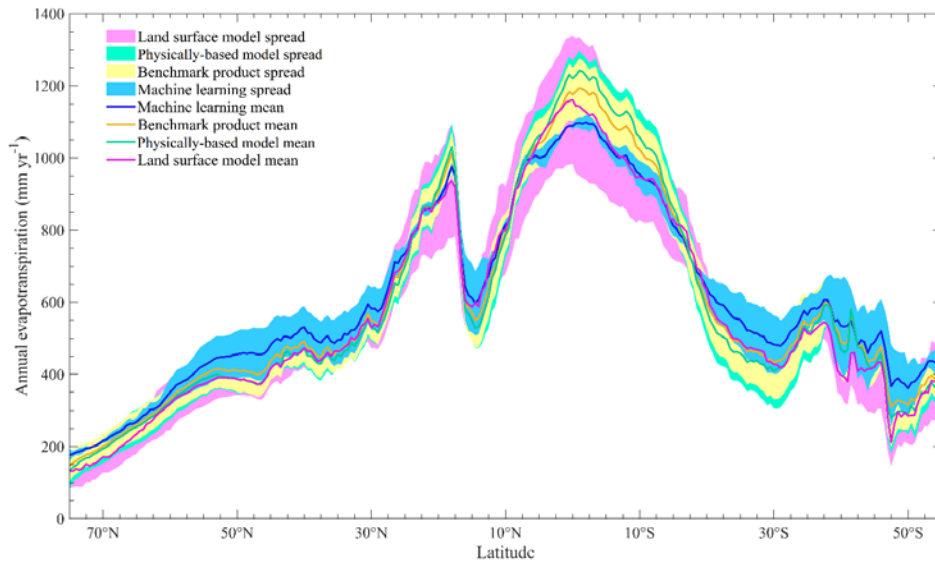
398 3.2 Spatial patterns of global terrestrial ET

399 As shown in Fig. 2, the spatial patterns of multi-year average annual ET ~~derived by of~~ different
400 ~~approaches categories~~ were similar. ET was the highest in the tropics and low in northern high
401 latitudes and arid regions such as Australia, central Asia, western U.S., and Sahel. Compared to
402 remote sensing-based physical models and LSMs, machine-learning methods obtained a smaller
403 spatial gradient. In general, latitudinal profiles of ET estimated by different approaches were also
404 consistent (Fig. 3). However, machine-learning methods gave higher ET estimate at high latitudes
405 and lower ET in the tropics compared to other approaches. In the tropics, LSMs have significant
406 larger uncertainties than benchmark products, and the standard deviation of LSMs is about two
407 times as large as that of benchmark products (Fig. 3). In other latitudes, LSMs and benchmark ET
408 products have generally comparable uncertainties. The largest difference in ET of different
409 categories was found in the Amazon Basin (Fig. 2). In most regions of the Amazon Basin, the
410 mean ET of remote sensing physical models are more than 200 mm yr^{-1} higher than the mean ET
411 of LSMs and machine-learning methods. For individual ET estimates, the largest uncertainty was
412 also found in the Amazon Basin. MODIS, VISIT and CLASS-CTEM estimated that annual ET
413 was larger than 1300 mm in the majority of Amazon, whereas JSBACH and LPJ-wsl estimated
414 ET of smaller than 800 mm yr^{-1} (Fig. S1). As is shown in Fig. S2, the differences in ET estimates
415 among TRENDY models were larger than those among benchmark estimates ~~in for~~ tropical and
416 humid regions. The uncertainty of ET estimates by LSMs is particularly large in the Amazon Basin
417 where the standard deviation of LSMs estimates is more than two times as large as that of

418 benchmark estimates. It is noteworthy that, in arid and semi-arid regions such as western Australia,
419 central Asia, northern China and western US, the differences in ET estimates among LSMs is
420 significantly smaller than those among remote sensing models and machine learning algorithms.



421
422 **Figure 2.** Spatial distributions of mean annual ET derived from (a) remote sensing-based physical
423 models, (b) machine-learning algorithms, (c) benchmark datasets and (d) TRENDY LSMs
424 ensemble mean, respectively.

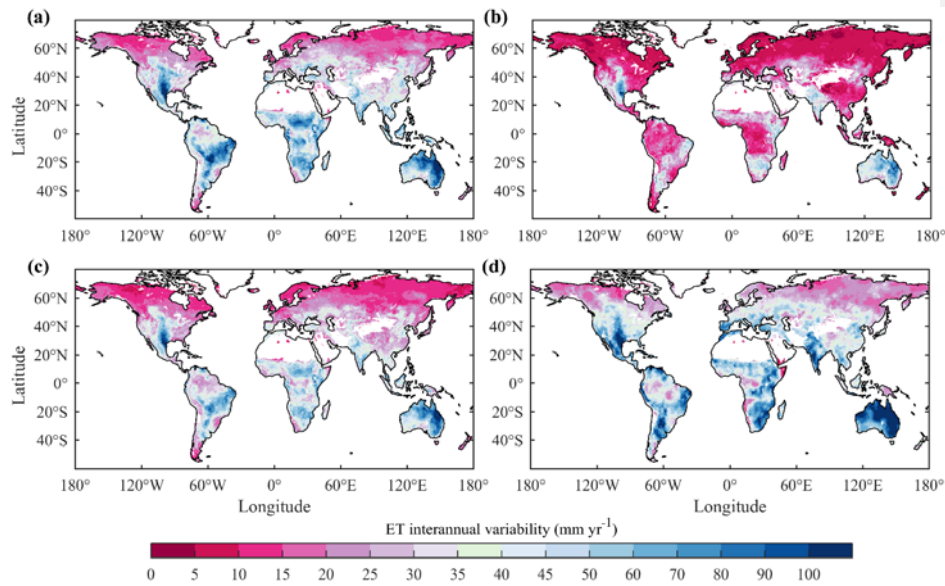


425
 426 **Figure 3.** Latitudinal profiles of mean annual ET for different categories of models. Each line
 427 represents the mean value of the corresponding category and the shading represents the interval of
 428 one standard deviation.

429 **3.3 Inter-annual variations in global terrestrial ET**

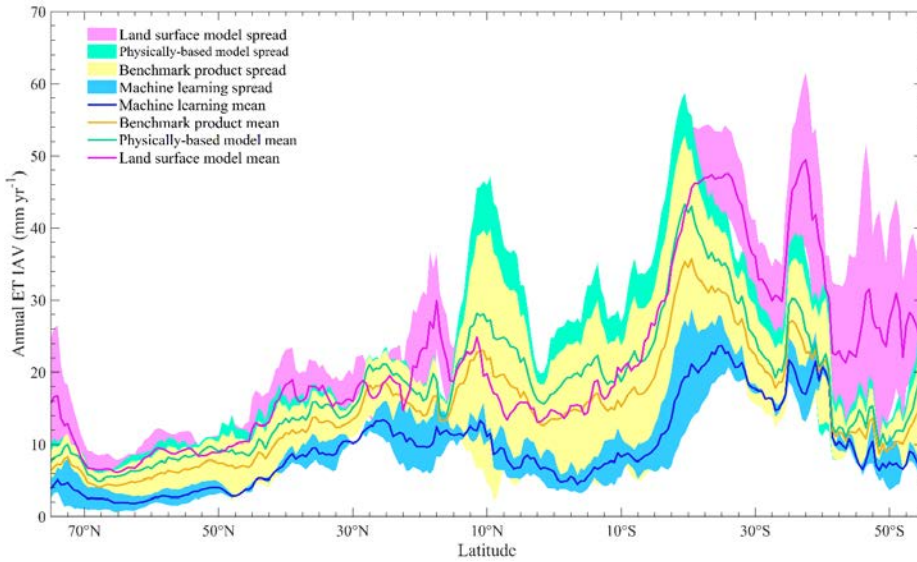
430 The ensemble mean inter-annual variability (IAV) of remote sensing ET estimates and LSMs ET
 431 estimates showed similar spatial patterns (Fig. 4). Both remote sensing physical models and LSMs
 432 presented low IAV in ET in northern high latitudes but high IAV in ET in southwestern U.S, India,
 433 south Sahara Africa, Amazon and Australia. In contrast, IAV of machine-learning based ET was
 434 much weaker. In most regions, IAV of machine learning ET is smaller than 40% of IAV of remote
 435 sensing physical ET and LSMs ET, and this phenomenon is especially pronounced in tropical
 436 regions. Further investigation into the spatial patterns of ET IAV for individual models showed
 437 that the two machine-learning methods performed equally in estimating spatial patterns of ET IAV

438 (Fig. S4). In contrast, differences in ET IAV among remote sensing physical estimates and LSMs
 439 estimates were much larger. LSMs showed the largest differences in IAV of ET in tropical regions.
 440 For example, CABLE and JULES obtained an ET IAV of smaller than 15 mm yr^{-1} in most regions
 441 of the Amazon Basin, while LPJ-GUESS predicted an ET IAV of larger than 60 mm yr^{-1} . Figure
 442 5 showed that, in the north of 20°S , remote sensing physical ET and LSMs ET had comparable
 443 IAV, but IAV of the machine learning based ET was much smaller. In the region south of 20°S ,
 444 TRENDY ET showed the largest IAV, followed by those of remote sensing physical ET and
 445 machine learning estimates. The three categories of models approaches agreed on that ET IAV in
 446 the Southern Hemisphere was generally larger than that in the Northern Hemisphere.



447
 448 **Figure 4.** Spatial distributions of the inter-annual variability in ET derived from (a) remote
 449 sensing-based physical models, (b) machine learning algorithms, (c) benchmark datasets, and (d)

450 TRENDY LSMs ensemble mean, respectively. The study period used in this study for inter-annual
451 variability analysis is from 1982 to 2011.



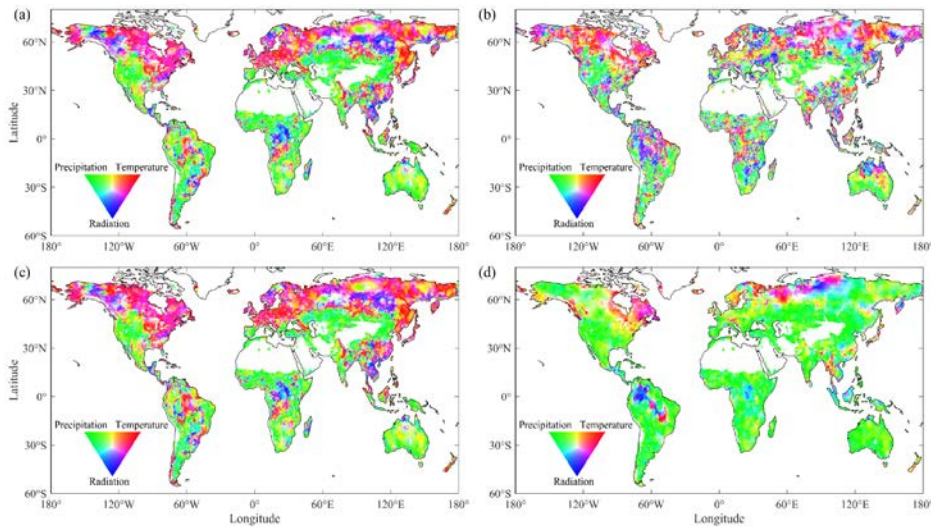
452
453 **Figure 5.** Latitudinal profiles of ET IAV for different categories of models. Each line represents
454 the mean value of the corresponding category and the shading represents the interval of one
455 standard deviation.

456 3.4 Climatic controls on ET

457 According to the ensemble remote sensing models, temperature and radiation dominated ET IAV
458 in ~~the~~ northern Eurasia, northern and eastern North America, southern China, the Congo River
459 Basin and the southern Amazon River Basin, while precipitation dominated ET IAV in arid regions
460 and semi-arid regions (Fig. 6a). The ensemble machine-learning algorithms had a similar pattern,
461 but suggested a stronger control of radiation in the Amazon Basin and a weaker control of

462 precipitation in several arid regions such as central Asia and northern Australia (Fig. 6b). In
463 comparison, the ensemble LSMs suggested the strongest control of precipitation on ET IAV (Fig.
464 6). According to the ensemble LSMs, ET IAV was dominated by precipitation IAV in most regions
465 of the Southern Hemisphere and northern low latitudes. Temperature and radiation only controlled
466 northern Eurasia, eastern Canada and part of the Amazon Basin (Fig. 6d). As is shown in Fig. S6,
467 the majority of LSMs agreed on the dominant role of precipitation in controlling ET in regions
468 south of 40°N. However, the pattern of climatic controls in the ORCHIDEE-MICT model is quite
469 unique and different from all other LSMs. According to the ORCHIDEE-MICT model, radiation
470 and temperature dominate ET IAVs in more regions, and precipitation only controls ET IAVs in
471 eastern Brazil, northern Russia, central Europe and a part of tropical Africa. Since ORCHIDEE-
472 MICT was developed from ORCHIDEE, the dynamic root parameterization in ORCHIDEE-MICT
473 may explain why ET is less driven by ~~Precipitation-precipitation~~ compared to ORCHIDEE (Haverd
474 et al., 2018). It is noted that two machine learning algorithms MTE and RF had significant
475 discrepancies in the spatial pattern of dominant climatic factors. According to the result of MTE,
476 temperature controlled ET IAV in regions north of 45°N, eastern US, southern China and the
477 Amazon basin (Fig. S6e). By contrast, RF suggested that precipitation and radiation dominated ET
478 IAV in these regions (Fig. S6f).

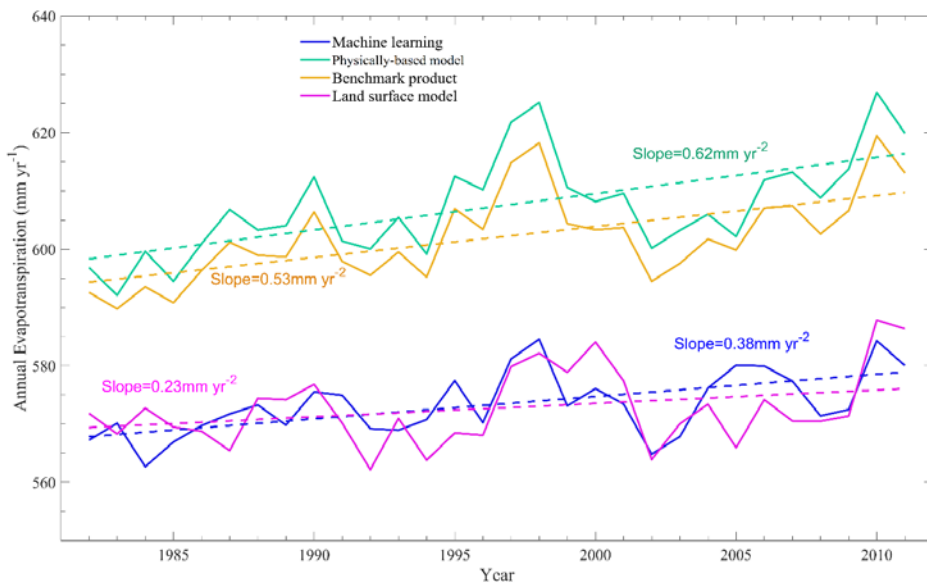
479



480
 481 **Figure 6.** Spatial distributions of climatic controls on inter-annual variation of ET derived from
 482 the ensemble means of remote sensing-based physical models (a), machine learning algorithms
 483 (b), benchmark data (c), and TRENDY LSMs (d). (red: temperature; green: precipitation; and blue:
 484 radiation).

485 3.5 Long-term trends in global terrestrial ET

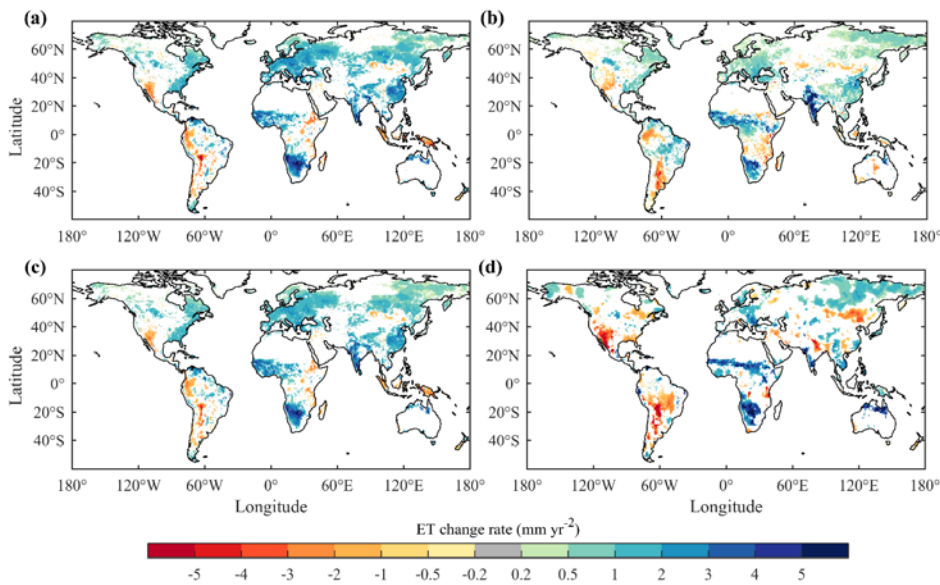
486 All approaches suggested an overall increasing trend in global ET during the period 1982-2011
 487 (Fig. 7), although ET decreased over 1998-2009. This result is consistent with previous studies
 488 (Jung et al., 2010; Lian et al., 2018; Zhang et al., 2015). Remote sensing physical models indicated
 489 the largest increase in ET (0.62 mm yr^{-2}), followed by the machine-learning method (0.38 mm yr^{-2}),
 490 and land surface models (0.23 mm yr^{-2}). Mean ET of all categories except ~~TRENDY~~
 491 ~~models~~ LSMs significantly increased during the study period ($p < 0.05$). It is noted that the ensemble
 492 mean ET of different categories are statistically correlated with each other ($p < 0.001$), even if the
 493 driving forces of different ET approaches are different.



494
 495 **Figure 7.** Inter-annual variations in global terrestrial ET estimated by different categories of
 496 approaches.

497 All remote sensing and machine learning estimates indicate a significant increasing positive trend
 498 in ET during the study period ($p < 0.05$), although the increase rate of P-LSH (1.07 mm yr^{-2}) is more
 499 than three times as large as that of GLEAM (0.33 mm yr^{-2}). Nevertheless, there is a larger
 500 discrepancy among LSMs in terms of ET trend. The majority of LSMs (10 of 14) suggest ~~an~~
 501 increasing a positive trend with the average trend of 0.34 mm yr^{-2} ($p < 0.05$), and eight of them are
 502 statistically significant (see Table 2). However, four LSMs (JSBACH, JULES, ORCHIDEE and
 503 ORCHIDEE-MICT) suggest a decreasing negative trend with the average trend of -0.12 mm yr^{-2}
 504 ($p > 0.05$). Among the four negative trends, and only the trend of ORCHIDEE-MICT (-0.34 mm
 505 yr^{-2}) is statistically significant ($p < 0.05$).

506 According to Fig. 8, the ensemble means of all the three approaches showed positive increasing
 507 trends of ET over western and southern Africa, western Indian, and northern Australia, and
 508 decreasing ET over western United States, southern South America and Mongolia. Discrepancies
 509 in ET trends mainly appeared in East Europe, eastern India and central China. LSMs also suggested
 510 larger area of decreasing ET in both North America and South America. Although the differences
 511 in ET trends among individual models were larger than that those among the ensemble means of
 512 different approaches, the majority of models agreed ~~on~~ that ET increased in western and southern
 513 Africa, and decreased in western United States and southern South America (Fig. S2). For both
 514 remote sensing estimates and LSMs estimates, ET trends in Amazon Basin had large uncertainty.
 515 P-LSH, CLM-45 and VISIT suggested large area of increasing ET, in contrast, GLEAM, JSBACH
 516 and ORCHIDEE suggested a large area of decreasing ET.



517

518 **Figure 8.** Spatial distributions of ET trends during the period 1982-2011 derived from (a) remote
519 sensing-based physical models, (b) machine learning algorithm, (c) benchmark datasets, and (d)
520 TRENDY LSMs ensemble mean, respectively. Regions with non-significant trends were
521 excluded.

522 3.6 Impacts of vegetation changes on ET variations

523 During the period 1982-2011, global LAI trends estimated from remote sensing data and from the
524 ensemble LSMs are $2.51 \times 10^{-3} \text{ m}^2 \text{ m}^{-2} \text{ yr}^{-1}$ ($p < 0.01$) and $4.63 \times 10^{-3} \text{ m}^2 \text{ m}^{-2} \text{ yr}^{-1}$ ($p < 0.01$), respectively
525 (Table 2). ~~Each~~ All LSMs suggested a significant ~~increasing-positive~~ trend in global LAI
526 (greening). It was found that, for both benchmark estimates and LSMs estimates, the spatial pattern
527 of trends in ET matched well with that of trends in LAI (Fig. ~~5e8c~~-d and Fig. S5a-b), indicating
528 significant effects of vegetation dynamics on ET variations. According to the results of multiple
529 linear regression, all models agreed ~~on~~ that greening of the Earth since the early 1980s intensified
530 terrestrial ET (Table 2), although there was a significant discrepancy in the magnitude of ET
531 intensification which varied from 0.04 mm yr^{-2} to 0.70 mm yr^{-2} . The ensemble LSMs suggested a
532 smaller ET increase (0.23 mm yr^{-2}) than the ensemble remote sensing physical models (0.62 mm
533 yr^{-2}) and machine-learning algorithm (0.38 mm yr^{-2}). Nevertheless, the greening-induced ET
534 intensification estimated by LSMs (0.37 mm yr^{-2}) is larger than that estimated by remote sensing
535 models (0.28 mm yr^{-2}) and machine-learning algorithms (0.09 mm yr^{-2}) because LSMs suggested
536 a stronger greening trend than remote sensing models. The contribution of vegetation greening to
537 ET intensification estimated by the ensemble LSMs is larger than 100% while ~~that-the~~
538 contributions estimated by the ensemble remote sensing physical models (0.62 mm yr^{-2}) and
539 machine-learning algorithm are smaller than 50%. Although TRENDY LSMs were driven by the
540 same climate data and remote sensing physical models were driven by varied climate data,

541 TRENDY LSMs still showed a larger discrepancy in terms of the effect of vegetation greening on
542 terrestrial ET than remote sensing physical models because of the significant differences in both
543 LAI trends ($1.74\text{-}13.63 \times 10^{-3} \text{ m}^2 \text{ m}^{-2} \text{ yr}^{-1}$) and the sensitivities of ET to LAI ($4.04\text{-}217.39 \text{ mm yr}^{-1}$
544 $\text{ per m}^2 \text{ m}^{-2}$). In comparison, remote sensing physical models had smaller discrepancies in terms
545 of the sensitivity of ET to LAI ($55.78\text{-}143.43 \text{ mm yr}^{-2} \text{ per m}^2 \text{ m}^{-2}$).

546 4. Discussion and perspectives

547 4.1 Sources of uncertainty

548 4.1.1 Uncertainty in the ET estimation of Amazon Basin

549 LSMs ~~have show~~ large discrepancies in the magnitude and trend of ET in the Amazon Basin (Fig.
550 3 and Fig. S3). However, it is challenging to identifying the uncertainty sources ~~is complex~~. Given
551 that the TRENDY LSMs used uniform meteorological inputs, the discrepancies in ET estimates
552 among ~~fferences~~ of the participating models mainly arise from the differences in underlying model
553 structures and parameters. One potential source of uncertainty is the parameterization of root water
554 uptake. In the Amazon Basin, large root depth was confirmed by field measurements (Nepstad et
555 al., 2004). However, many LSMs have an unrealistically small rooting depth (generally less than
556 2 m), neglecting the existence and significance of deep roots. The incorrect root distributions
557 enlarge the differences in plant available water and root water uptake, producing large
558 uncertainties in ET. In addition, differences in the parameterization of other key processes
559 pertinent to ET such as LAI dynamics (Fig. S5), canopy conductance variations (Table 1), water
560 movements in the soil (Abramopoulos et al., 1988; Clark et al., 2015; Noilhan and Mahfouf, 1996)
561 and soil moisture's control on transpiration (Purdy et al., 2018; Szutu and Papuga, 2019) also
562 increase the uncertainty in ET. The above-mentioned processes are not independent of each other
563 but interact in complex ways to produce the end result.

564 4.1.2 Uncertainty in the ET estimation of arid and semi-arid regions

565 In arid and semi-arid regions, benchmark products show much larger differences in the magnitude
566 of ET than LSMs (Fig. S2). One cause of this phenomenon is the differences in meteorological
567 forcing. Remote sensing and machine learning datasets used different forcing data. For
568 precipitation, RF used [the CRUNCEPv6 dataset](#); MTE used [the Global Precipitation Climatology](#)
569 [Centre \(GPCC\) dataset](#); MODIS used [the Global Modeling and Assimilation Office \(GMAO\)](#)
570 [dataset](#); GLEAM used [the Multi-Source Weighted-Ensemble Precipitation \(MSWEP\) dataset](#);
571 PML-CSIRO used the Princeton Global Forcing (PGF) and the WATCH Forcing Data ERA-
572 Interim (WFDEI) datasets; and P-LSH used data derived from four independent sources. Since
573 precipitation is the key climatic factor controlling ET in arid and semi-arid regions (Fig. 6),
574 discrepancies between different forcing precipitation (Sun et al., 2018) may be the main source of
575 large uncertainty there. In comparison, the uniform forcing data reduced the inter-model range in
576 ET estimates of TRENDY LSMs. Nevertheless, it is noted that the congruence across LSMs ET
577 estimates doesn't necessarily mean they are the correct representation of ET. The narrower inter-
578 model range may suggest shared biases. All remote sensing models and machine learning
579 algorithms except GLEAM do not explicitly take the effects of soil moisture into account (Table
580 S1). Given that soil moisture is pivotal to both canopy conductance and soil evaporation in arid
581 and semi-arid regions (A et al., 2019; De Kauwe et al., 2015; Medlyn et al., 2015; Purdy et al.,
582 2018), the lack of soil moisture information also increases the bias in ET estimation. In addition,
583 the accuracy of remotely-sensing data itself is also an uncertainty source. The retrieval of key land
584 surface variables, such as leaf area index and surface temperature, is influenced by vegetation
585 architecture, solar zenith angle and satellite observational angle, particularly over heterogeneous
586 surface (Norman and Becker, 1995).

587 4.1.3 Uncertainty in the ET IAV in the Southern Hemisphere

588 In regions south of 20°S (including Australia, southern Africa and southern South America), the
589 ET IAVs of remote sensing models and machine learning algorithms are smaller than that of LSMs
590 (Fig. 4 and 5), although their spatial patterns are similar. In these regions, GLEAM, the only remote
591 sensing model ~~that~~ explicitly considers the effects of soil moisture, has larger ET IAVs than other
592 remote sensing models and has similar ET IAVs with LSMs (Fig. S4). ~~It implies~~ This could imply
593 that most existing remote sensing models may underestimate ET IAVs in the Southern Hemisphere
594 because the effects of soil moisture ~~is-are~~ not explicitly considered. Machine learning algorithms
595 ~~have-show~~ much smaller IAVs than other models (Fig. 4 and S4). The main reason is that ET inter-
596 annual variability is partly neglected in the training process because the magnitude of ET inter-
597 annual variability is usually smaller than the spatial and seasonal variability (Anav et al., 2015;
598 Jung et al., 2019). Moreover, the IAV of satellite-based key land surface variables such as LAI,
599 fAPAR and surface temperature may be not reliable because of the effects of clouds, which also
600 affects the estimation of IAV of satellite-based ET. It is noted that LSMs ET IAVs show large
601 differences in latitudes south of 20°S (Fig. 5). This divergence in ET IAV indicates that ~~land~~
602 ~~surface models~~ LSMs need better representation of ET response to climate in the Southern
603 Hemisphere.

604

605 4.1.4 Uncertainty in global ET trend

606 All ~~of~~ the three categories of ET models detected an overall ~~increasing-positive~~ trend in global
607 terrestrial ET since the early 1980s, which is in agreement with previous studies (Mao et al., 2015;
608 Miralles et al., 2014; Zeng et al., 2018a; Zeng et al., 2018b; Zeng et al., 2014; Zhang et al., 2015;
609 Zhang et al., 2016b). Benchmark products generally suggested stronger ET intensification than

610 LSMs. The weaker ET intensification in LSMs may be induced by the response of stomatal
611 conductance to increasing atmospheric CO₂ concentration. The increasing CO₂ affects ET in two
612 ways. On one hand, increasing CO₂ can effectively reduce stomatal conductance and thus decrease
613 transpiration (Heijmans et al., 2001; Leipprand and Gerten, 2006; Swann et al., 2016); on the other
614 hand, it can increase vegetation productivity and thus increase LAI. For benchmarks, the second
615 effect could be captured by remotely sensed LAI, NDVI or fAPAR, while the first effect was
616 neglected by all models except P-LSH (Zhang et al., 2015). In contrast, both effects were modeled
617 in all TRENDY LSMs.

618 LAI dynamics have significant influences on ET. The increased LAI trend (greening) since the
619 early 1980s was reported by previous studies (Mao et al., 2016; Zhu et al., 2016) and is also
620 confirmed by remote sensing data and all TRENDY LSMs used in this study (Table 2 and Fig.
621 S5). Zhang et al. (2015) found that the ~~increasing-positive~~ trend of global terrestrial ET over 1982-
622 2013 was mainly driven by ~~an~~ increase in LAI and the enhanced atmosphere water demand. Using
623 a land-atmosphere coupled global climate model (GCM), Zeng et al. (2018b) further estimated
624 that global LAI increased about 8%, resulting in an increase of $0.40 \pm 0.08 \text{ mm yr}^{-1}$ in global ET
625 (contributing to $55\% \pm 25\%$ of the ET increase). This number is close to the estimates of ensemble
626 LSMs ($0.37 \pm 0.18 \text{ mm yr}^{-1}$). In comparison, remote sensing models and machine learning
627 algorithms used in this study suggested smaller greening-induced ET increases. It is noted that
628 TRENDY LSMs still showed a larger discrepancy in terms of the effect of vegetation greening on
629 terrestrial ET than remote sensing physical models (Table 2) because of the significant differences
630 in LAI trend ($1.74\text{-}13.63 \times 10^{-3} \text{ m}^2 \text{ m}^{-2} \text{ yr}^{-1}$) and in the sensitivity of ET to LAI ($4.04\text{-}217.39 \text{ mm}$
631 yr^{-2} per $\text{m}^2 \text{ m}^{-2}$). Uncertainties in LAI trend may arise from inappropriate carbon allocations and
632 deficits in responding to water deficits (Anav et al., 2013; Hu et al., 2018; Murray-Tortarolo et al.,

633 2013; Restrepo - Coupe et al., 2017). Additionally, for machine-learning algorithms, the results
634 from insufficient long-term in situ measurements and sparse observations in tropical, boreal and
635 arid regions imply that there likely are deficiencies in representing the temporal variations.

636 **4.1.5 Ignorance-Lack of knowledge of the effects of irrigation**

637 Irrigation accounts for about 90% of human consumptive water use and largely ~~affects~~ ET in
638 irrigated croplands (Siebert et al., 2010). Global water withdrawals for irrigation ~~were~~
639 estimated to be within the range of 1161-3800 km³-yr⁻¹ around the year 2000, and largely increased
640 during the period 2000-2014 (Chen et al., 2019). However, none of the remote sensing-based
641 physical models and machine-learning algorithms explicitly accounted for the effects of irrigation
642 on ET, although these effects could be taken into account to some extent by using observed LAI,
643 NDVI, or fAPAR to drive the models (Zhang et al., 2015). Considering that annual ET may surpass
644 annual precipitation in cropland, Zhang et al. (2016b) used the Budyko hydrometeorological model
645 to constrain PML-CSIRO model only in grids covered by non-crop vegetation. But the process of
646 irrigation affecting evaporation was still not taken into consideration. For TRENDY LSMs, only
647 2 of 14 models (DLEM and ISAM) included the irrigation processes (Le Quéré et al., 2018).
648 Therefore, the effects of irrigation are largely neglected in existing global ET datasets, which
649 reduces the accuracy of local ET estimates in regions with a large proportion of irrigated cropland.

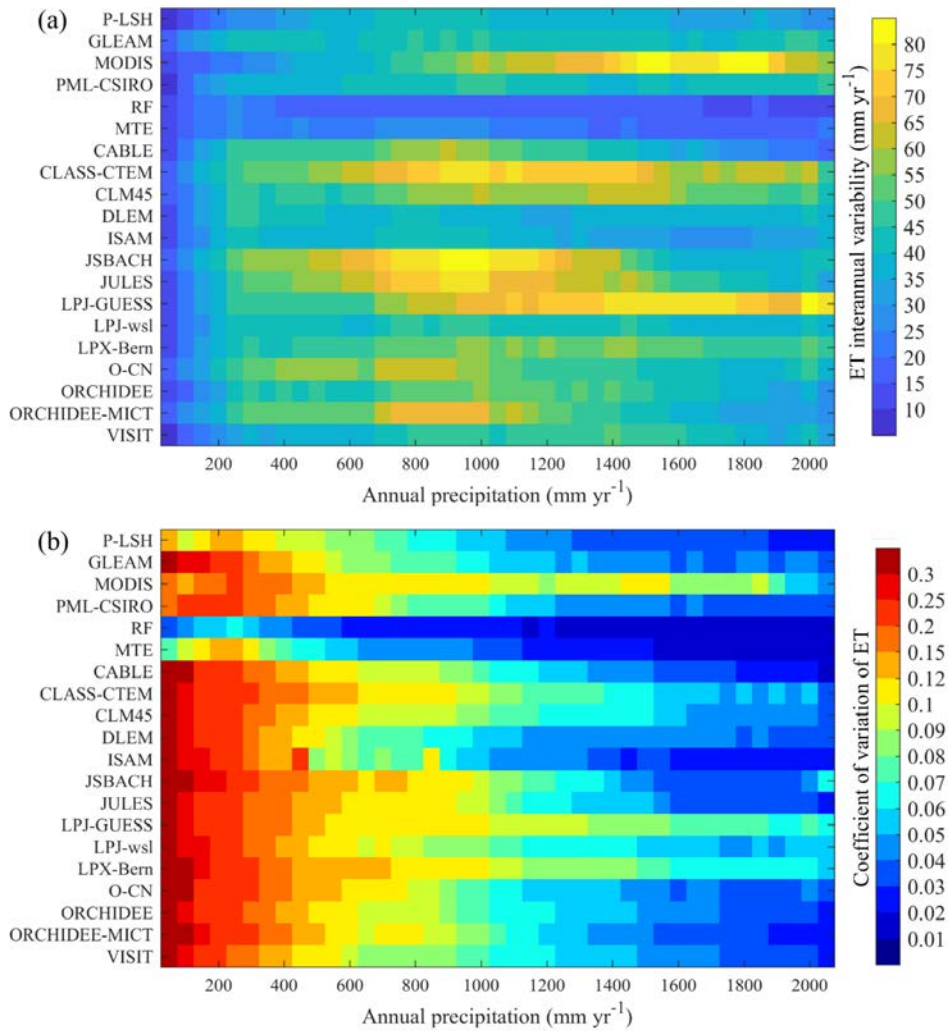
650 **4.1.6 ET variability across precipitation gradient and its planetary boundary**

651 Precipitation is the source of terrestrial evapotranspiration. According to Fig. 9a, the vast majority
652 of models agree that ET has the largest IAV in regions with annual precipitation between 700 mm
653 and 1000 mm, although the magnitude of ET IAV has substantial discrepancies among different
654 models. The low ET IAV in arid and semi-arid regions doesn't mean ET is stable in these regions.
655 In fact, ET has the largest coefficient of variation (CoV, the ratio of ET standard deviation to ET

556 mean value) in arid regions, and all models show a clear negative trend of CoV with increasing
557 precipitation (Fig. 9b). This is mainly caused by the large CoV of precipitation in arid regions
558 (Fatichi et al., 2012).

559 In comparison, terrestrial ET shows a much smaller IAV at the global scale (Table 2), ranging
560 from 4.8 to 12.2 mm yr⁻¹ (one standard deviation), which only equals to 1.0-1.8% of global annual
561 mean ET. The model results suggest that global terrestrial ET stabilizes at about 6.74×10⁴ km³ yr
562 ¹ (603 mm yr⁻¹), which is close to previous estimates (Alton et al., 2009; Mueller et al., 2011; Oki
563 and Kanae, 2006; Zeng et al., 2012).The stability of global terrestrial ET is probably based on
564 partitioning the solar constant and suggests that, at a global scale, droughts in one place are
565 balanced by excess rain in other places so it all evens out. It implies that ET also has a potential
566 planetary boundary, a suggestion made by Running (2012) on NPP as a planetary boundary. ET
567 integrates four aspects of the current planetary boundaries defined by Steffen et al. (2015): climate
568 change, freshwater use, land-system change, and biochemical flows. Given ET's importance in
569 linking terrestrial water, carbon, nutrient and energy cycles, more studies on the ET planetary
570 boundary are needed under the background of intensifying global change and increasing human
571 perturbations on the Earth system.

Formatted: Superscript



672
 673 **Figure 9. Interannual variability (a) and coefficient of variation (b) of ET in each 50mm**
 674 **interval of mean annual precipitation.**

675 In short, the multi-model inter-comparison indicates that considerable uncertainty exists in both
 676 the temporal and spatial variations in global ET estimates, even though a large portion of models

677 adopt similar ET algorithms (Table 1). The major uncertainty source ~~could be~~ different for
678 different types of models and regions. The uncertainty is induced by multiple factors, including
679 problems pertinent to parameterization of land processes, lack of in situ measurements, remote
680 sensing acquisition, scaling effects and meteorological forcing. Based on the results of different
681 approaches, we suggest that global terrestrial ET also has a potential planetary boundary, with the
682 value being about $6.74 \times 10^4 \text{ km}^3 \text{ yr}^{-1}$ (603 mm yr^{-1}), which is consistent with previous estimates.

683 **4.2 Recommendations for future development**

684 **4.2.1 Remote sensing-based physical methods**

685 In the past decades, the development of remote sensing technologies has contributed to the boom
686 of various ET estimating methods. However, there is still a large room for remote sensing
687 technologies to improve (Fisher et al., 2017). Developing new platforms and sensors that have
688 improved global spatiotemporal coverage and using multi-band, multi-source remote sensing data
689 are the key points. Planned or newly launched satellites, such as NASA's GRACE Follow-On
690 (GRACE-FO) mission and ECOSystem Spaceborne Thermal Radiometer Experiment on Space
691 Station (ECOSTRESS) mission, will improve the accuracy of terrestrial ET estimates.
692 ECOSTRESS's thermal infrared (TIR) multispectral scanner is capable of monitoring diurnal
693 temperature patterns at high-resolutions, which gives insights into plant response to water stress
694 and the means to understand sub-daily ET dynamics (Hulley et al.). GRACE Follow-On
695 observations can be used to constrain subsurface lateral water transfers, which helps to correct soil
696 moisture and subsequently improves the accuracy of ET estimates (Rouholahnejad and Martens,
697 2018). Moreover, building integrated methods that fuse different ET estimates or the upstream
698 satellite-based biophysical variables from different platforms and the other forcing data will be

699 helpful to improve the accuracy and spatiotemporal coverage of ET (Ke et al., 2016; Ma et al.,
700 2018; Semmens et al., 2016).

701 The theories and retrieval algorithms of ET and related key biophysical variables also need to be
702 further improved. For example, the method for canopy conductance calculation may be improved
703 by integrating remote sensing based solar-induced chlorophyll fluorescence (SIF) data. SIF data
704 in existing Global Ozone Monitoring Experiment-2 (GOME-2), Orbiting Carbon Observatory-2
705 (OCO-2) and TROPOspheric Monitoring Instrument (TROPOMI) and the forthcoming OCO-3
706 and Geostationary Carbon Cycle Observatory (GeoCarb) satellites provide a good opportunity for
707 diagnosing transpiration and for ET partitioning at multiple spatiotemporal scales (Pagán et al.,
708 2019; Stoy et al., 2019; Sun et al., 2017). Theoretical advancements in nonequilibrium
709 thermodynamics and Maximum Entropy Production (MEP) could be incorporated into the
710 classical ET theories (Xu et al., 2019; Zhang et al., 2016a). In addition, quantifying the effects of
711 CO₂ fertilization on stomatal conductance is pivotal for remote sensing models to capture the long-
712 term trend of terrestrial ET.

713 Most existing remote sensing-based ET studies focused on total ET, however, the partitioning of
714 ET between transpiration, soil evaporation, and canopy interception may have significant
715 divergence even though the total ET is accurately estimated (Talsma et al., 2018b). In current
716 remote sensing-based ET models, soil evaporation, which is sensitive to precipitation events and
717 soil moisture, is the part with the largest error (Talsma et al., 2018a). Therefore incorporating the
718 increasing accessible satellite-based precipitation, soil moisture observations and soil property
719 data will contribute to the improvement of soil evaporation estimation. Meanwhile, the
720 consideration of soil evaporation under herbaceous vegetation and canopy will also reduce the
721 errors.

Formatted: Font color: Text 1

Formatted: Font color: Text 1

Formatted: Font color: Text 1

Formatted: Font color: Text 1

Formatted: Font color: Text 1

722 4.2.2 Machine learning methods

723 It is well known that the capability of machine-learning algorithms in providing accurate ET
724 estimates largely depends on the representativeness of training datasets in describing ecosystem
725 behaviors (Yao et al., 2017). As a result, machine-learning algorithms may not perform well
726 outside the range of the data used for their training. Unfortunately, long-term field observations
727 out of northern temperate regions are still insufficient; ~~T~~h~~i~~~~s~~ ~~i~~~~s~~ ~~a~~~~n~~ ~~i~~~~m~~~~p~~~~o~~~~r~~~~t~~~~a~~~~n~~~~c~~~~e~~ ~~f~~~~o~~~~r~~
728 ~~o~~~~f~~ the small spatial gradient and small IAVs of machine-learning ET. Given that remote sensing
729 is capable of providing broad coverage of key biophysical variables at reasonable spatial and
730 temporal resolutions, one way to overcome this challenge is to exclusively use remote sensing
731 observations as training data (Jung et al., 2019; Poon and Kinoshita, 2018). Another simple way
732 to make IAVs of machine-learning ET more realistic is normalizing the yearly anomalies when
733 comparing with ET estimates from LSMs and remote sensing physical models (Jung et al., 2019).
734 New machine-learning techniques, including the extreme learning machine and the adaptive
735 neuro-fuzzy inference system, can be used to improve the accuracy of ET estimation (Gocic et al.,
736 2016; Kişi and Tombul, 2013). The emerging deep learning methods such as recurrent neural
737 network (RNN) and Long Short-Term Memory (LSTM) have large potential to outcompete
738 conventional machine-learning methods in modelling ET time series (Reichstein et al., 2018;
739 Reichstein et al., 2019). Almost all machine-learning datasets used precipitation rather soil
740 moisture as explanatory variable when training. However, soil moisture rather than precipitation
741 directly controls ET. As more and more global remote sensing based soil moisture datasets become
742 available, using soil moisture products as input is expected to improve the accuracy of ET
743 estimates, especially for regions with ~~s~~~~p~~~~a~~~~r~~~~s~~ ~~s~~~~p~~~~a~~~~r~~~~s~~e vegetation coverage (Xu et al., 2018).

744 4.2.3 Land surface models

745 In contrast to observation-based methods, LSMs are able to ~~predict-project~~ future changes in ET,
746 and can disentangle the effects of different drivers on ET through factorial analysis. However,
747 results from LSMs are only as good as their parameterizations of complex land surface processes
748 which are limited by our incomplete understanding of physical and biological processes (Niu et
749 al., 2011). Although TRENDY LSMs are the ~~state-of-the-art~~state-of-the-art process-based global
750 land surfaces models, improvements are still needed because several important processes are
751 missing or not being appropriately parameterized. Most of the TRENDY LSMs did not simulate
752 the processes relevant to human management including irrigation (Chen et al., 2019) and
753 ~~fertilization-application of fertilizers~~ (Mao et al., 2015), and natural disturbances like wildfire
754 (Poon and Kinoshita, 2018). Incorporating these processes into present LSMs is critical, ~~although~~
755 ~~However, we need to keep it in mind that these processes should be added with caution, because~~
756 ~~adding more processes and introducing introduction of~~ new model parameters ~~may potentially also~~
757 leads to an increase in a model's uncertainty.

758 In light of the importance of soil water availability in constraining canopy conductance and
759 dynamics, accurate representation of hydrological processes is a core task for LSMs, particularly
760 in dry regions. Integrating a dynamic root water uptake function and hydraulic redistribution into
761 the LSM can significantly improve its performance of estimating seasonal ET and soil moisture
762 (Li et al., 2012). Moreover, other hydrological processes including groundwater (Decker, 2015),
763 lateral flow (Rouholahnejad and Martens, 2018) and water vapor diffusion at the soil surface
764 (Chang et al., 2018) need to be simulated and correctly represented to reproduce the dynamics of
765 soil water and ET. Since canopy LAI plays an important role in regulating ET, correctly simulating
766 vegetation dynamics is also critical. One way is to correct the initialization, distribution, and
767 parameterization of vegetation phenology in LSMs (Murray-Tortarolo et al., 2013; Zhang et al.,

768 2019). Appropriate carbon allocation scheme and parameterization of vegetation's response to
769 water deficits are also important for reproducing vegetation dynamics (Anav et al., 2013).

770 **5. Conclusion**

771 In this study, we evaluated twenty global terrestrial ET estimates including four from remote
772 sensing-based physical models, two from machine-learning algorithms and fourteen from
773 TRENDY LSMs. The ensemble mean values of global terrestrial ET for the three categories agreed
774 well, ranging from 589.6 mm yr⁻¹ to 617.1 mm yr⁻¹. All ~~of~~ the three categories detected an overall
775 increasing-positive trend in global ET during the period 1982-2011 and suggested a positive effect
776 of vegetation greening on ET intensification. However, the multi-model inter-comparison
777 indicates that, considerable uncertainties still exist in both ~~the~~ temporal and spatial variations in
778 global ET estimates. LSMs had significant differences in the ET magnitude in tropical regions
779 especially the Amazon Basin, while benchmark ET products showed larger inter-model range in
780 arid and semi-arid regions than LSMs. Trends in LSMs ET estimates also had significant
781 discrepancies. These uncertainties are induced by parameterization of land processes,
782 meteorological forcing, lack of in situ measurements, remote sensing acquisition and scaling
783 effects. Model developments and observational improvements provide two parallel pathways
784 towards improving the accuracy of global terrestrial ET estimation.

785 **Code and data availability**

786 TRENDYv6 data are available from S.S. (s.a.sitch@exeter.ac.uk) on reasonable request. MODIS
787 ET data are available from http://files.ntsug.umt.edu/data/NTSG_Products/MOD16/. GLEAM ET
788 are available from <https://www.gleam.eu/>. Both Model Tree Ensemble and Random Forest ET are
789 available from <https://www.bgc-jena.mpg.de/geodb/projects/FileDetails.php>. P-LSH ET are

790 available from http://files.nts.g.umd.edu/data/ET_global_monthly/Global_8kmResolution/.
791 PML-CSIRO ET are from <https://data.csiro.au/dap/landingpage?pid=csiro:17375>. CRU-
792 NCEPv8 data are available from Nicolas Viovy on reasonable request. GIMMS LAI3gV1 data are
793 available from R. B. Myneni on reasonable request. GIMMS NDVI3gV1 data are available from
794 <https://ecocast.arc.nasa.gov/data/pub/gimms/3g.v1/>.

795 **Author contributions**

796 S.P. initiated this research and was responsible for the integrity of the work as a whole. N.P. carried
797 out the analyses. S.P., N.P., H.T. and H.S. wrote the manuscript with contributions from all
798 authors. P.F., S.S., V.K.A., V.H., A.K.J., E.K., S.L., D.L., J.E.M.S.N., C.O., B.P., H.T. and S.Z.
799 contributed to the TRENDY results.

800 **Competing interests**

801 The authors declare that they have no conflict of interest.

802 **Acknowledgements**

803 This study has been supported partially by grants from National Science Foundation (1903722 and
804 1243232), AU-OUC Joint Center Program and Auburn University IGP Program. ~~Atul K~~
805 ~~Jain A.K.J.~~ was support in part by Department of Energy (No. DE - SC0016323) and NSF (NSF
806 AGS 12-43071). D.L. acknowledges funding from the National Institute of Food and
807 Agriculture/US Department of Agriculture (2015- 67003-23489 and 2015-67003-23485). S.L.
808 acknowledges support from EC H2020 (CCiCC; grant no 821003) and SNSF (grant no.
809 20020_172476). ~~Vanessa Haverd~~ V.H. acknowledges support from the Earth Systems and Climate
810 Change Hub, funded by the Australian Government's National Environmental Science Program.

811 We thank all people who provided data used in this study, in particular, the TRENDY modelling
812 [groups.](#) [Additional details on funding support for the participating 14 land surface models have](#)
813 [been provided in the TRENDY Project.](#)

814

815 **References**

- 816 A, Y., Wang, G., Liu, T., Xue, B., and Kuczera, G.: Spatial variation of correlations between
817 vertical soil water and evapotranspiration and their controlling factors in a semi-arid region,
818 *Journal of Hydrology*, 574, 53-63, 2019.
- 819 Abramopoulos, F., Rosenzweig, C., and Choudhury, B.: Improved ground hydrology calculations
820 for global climate models (GCMs): Soil water movement and evapotranspiration, *Journal of*
821 *Climate*, 1, 921-941, 1988.
- 822 Allen, R. G., Pereira, L. S., Raes, D., and Smith, M.: Crop evapotranspiration-Guidelines for
823 computing crop water requirements-FAO Irrigation and drainage paper 56, Fao, Rome, 300,
824 D05109, 1998.
- 825 Alton, P., Fisher, R., Los, S., and Williams, M.: Simulations of global evapotranspiration using
826 semiempirical and mechanistic schemes of plant hydrology, *Global biogeochemical cycles*, 23,
827 2009.
- 828 Anav, A., Friedlingstein, P., Beer, C., Ciais, P., Harper, A., Jones, C., Murray - Tortarolo, G.,
829 Papale, D., Parazoo, N. C., and Peylin, P.: Spatiotemporal patterns of terrestrial gross primary
830 production: A review, *Reviews of Geophysics*, 53, 785-818, 2015.
- 831 Anav, A., Murray-Tortarolo, G., Friedlingstein, P., Sitch, S., Piao, S., and Zhu, Z.: Evaluation of
832 land surface models in reproducing satellite Derived leaf area index over the high-latitude
833 northern hemisphere. Part II: Earth system models, *Remote Sensing*, 5, 3637-3661, 2013.
- 834 Antonopoulos, V. Z., Gianniou, S. K., and Antonopoulos, A. V.: Artificial neural networks and
835 empirical equations to estimate daily evaporation: application to lake Vegoritis, Greece,
836 *Hydrological Sciences Journal*, 61, 2590-2599, 2016.
- 837 Barman, R., Jain, A. K., and Liang, M.: Climate - driven uncertainties in modeling terrestrial
838 energy and water fluxes: a site - level to global - scale analysis, *Global change biology*, 20,
839 1885-1900, 2014.
- 840 Bodesheim, P., Jung, M., Gans, F., Mahecha, M. D., and Reichstein, M.: Upscaled diurnal cycles
841 of land-atmosphere fluxes: a new global half-hourly data product, *Earth Syst. Sci. Data*, 10,
842 1327-1365, 2018.
- 843 Breiman, L.: Random forests, *Machine learning*, 45, 5-32, 2001.
- 844 Chang, L.-L., Dwivedi, R., Knowles, J. F., Fang, Y.-H., Niu, G.-Y., Pelletier, J. D., Rasmussen, C.,
845 Durcik, M., Barron-Gafford, G. A., and Meixner, T.: Why Do Large-Scale Land Surface Models
846 Produce a Low Ratio of Transpiration to Evapotranspiration?, *Journal of Geophysical Research:*
847 *Atmospheres*, 123, 9109-9130, 2018.
- 848 Chen, Y., Feng, X., Fu, B., Shi, W., Yin, L., and Lv, Y.: Recent global cropland water consumption
849 constrained by observations, *Water Resources Research*, 2019. 2019.

850 Chen, Y., Xia, J., Liang, S., Feng, J., Fisher, J. B., Li, X., Li, X., Liu, S., Ma, Z., and Miyata, A.:
851 Comparison of satellite-based evapotranspiration models over terrestrial ecosystems in China,
852 Remote Sensing of Environment, 140, 279-293, 2014.

853 Clark, M. P., Fan, Y., Lawrence, D. M., Adam, J. C., Bolster, D., Gochis, D. J., Hooper, R. P., Kumar,
854 M., Leung, L. R., and Mackay, D. S.: Improving the representation of hydrologic processes in
855 Earth System Models, Water Resources Research, 51, 5929-5956, 2015.

856 Cleugh, H. A., Leuning, R., Mu, Q., and Running, S. W.: Regional evaporation estimates from flux
857 tower and MODIS satellite data, Remote Sensing of Environment, 106, 285-304, 2007.

858 d'Orgeval, T., Polcher, J., and Rosnay, P. d.: Sensitivity of the West African hydrological cycle in
859 ORCHIDEE to infiltration processes, Hydrology and Earth System Sciences, 12, 1387-1401, 2008.

860 Dai, A.: Precipitation characteristics in eighteen coupled climate models, Journal of Climate, 19,
861 4605-4630, 2006.

862 De Kauwe, M. G., Kala, J., Lin, Y.-S., Pitman, A. J., Medlyn, B. E., Duursma, R. A., Abramowitz, G.,
863 Wang, Y., and Gonzalez Miralles, D.: A test of an optimal stomatal conductance scheme within
864 the CABLE land surface model, Geoscientific Model Development, 8, 431-452, 2015.

865 Decker, M.: Development and evaluation of a new soil moisture and runoff parameterization
866 for the CABLE LSM including subgrid - scale processes, Journal of Advances in Modeling Earth
867 Systems, 7, 1788-1809, 2015.

868 Dou, X. and Yang, Y.: Evapotranspiration estimation using four different machine learning
869 approaches in different terrestrial ecosystems, Computers and Electronics in Agriculture, 148,
870 95-106, 2018.

871 Douville, H., Ribes, A., Decharme, B., Alkama, R., and Sheffield, J.: Anthropogenic influence on
872 multidecadal changes in reconstructed global evapotranspiration, Nature Climate Change, 3,
873 59, 2013.

874 Famiglietti, J. and Wood, E. F.: Evapotranspiration and runoff from large land areas: Land
875 surface hydrology for atmospheric general circulation models, Surveys in Geophysics, 12, 179-
876 204, 1991.

877 Fatichi, S., Ivanov, V. Y., and Caporali, E.: Investigating Interannual Variability of Precipitation at
878 the Global Scale: Is There a Connection with Seasonality?, Journal of Climate, 25, 5512-5523,
879 2012.

880 Feng, Y., Cui, N., Gong, D., Zhang, Q., and Zhao, L.: Evaluation of random forests and generalized
881 regression neural networks for daily reference evapotranspiration modelling, Agricultural
882 Water Management, 193, 163-173, 2017.

883 Fisher, J. B., Malhi, Y., Bonal, D., Da Rocha, H. R., De Araujo, A. C., Gamo, M., Goulden, M. L.,
884 Hirano, T., Huete, A. R., and Kondo, H.: The land-atmosphere water flux in the tropics, Global
885 Change Biology, 15, 2694-2714, 2009.

886 Fisher, J. B., Melton, F., Middleton, E., Hain, C., Anderson, M., Allen, R., McCabe, M. F., Hook, S.,
887 Baldocchi, D., and Townsend, P. A.: The future of evapotranspiration: Global requirements for
888 ecosystem functioning, carbon and climate feedbacks, agricultural management, and water
889 resources, Water Resources Research, 53, 2618-2626, 2017.

890 Fisher, J. B., Tu, K. P., and Baldocchi, D. D.: Global estimates of the land-atmosphere water flux
891 based on monthly AVHRR and ISLSCP-II data, validated at 16 FLUXNET sites, Remote Sensing of
892 Environment, 112, 901-919, 2008.

893 Fu, B. P.: On the calculation of the evaporation from land surface, *Sci. Atmos. Sin*, 5, 23-31,
894 1981.

895 Fu, G., Charles, S. P., and Yu, J.: A critical overview of pan evaporation trends over the last 50
896 years, *Climatic change*, 97, 193, 2009.

897 Gedney, N., Cox, P., Betts, R., Boucher, O., Huntingford, C., and Stott, P.: Detection of a direct
898 carbon dioxide effect in continental river runoff records, *Nature*, 439, 835, 2006.

899 Glenn, E. P., Nagler, P. L., and Huete, A. R.: Vegetation index methods for estimating
900 evapotranspiration by remote sensing, *Surveys in Geophysics*, 31, 531-555, 2010.

901 Gocic, M., Petković, D., Shamshirband, S., and Kamsin, A.: Comparative analysis of reference
902 evapotranspiration equations modelling by extreme learning machine, *Computers and
903 Electronics in Agriculture*, 127, 56-63, 2016.

904 Good, S. P., Noone, D., and Bowen, G.: Hydrologic connectivity constrains partitioning of global
905 terrestrial water fluxes, *Science*, 349, 175-177, 2015.

906 Guimberteau, M., Zhu, D., Maignan, F., Huang, Y., Chao, Y., Dantec-Nédélec, S., Ottlé, C., Jornet-
907 Puig, A., Bastos, A., and Laurent, P.: ORCHIDEE-MICT (v8. 4.1), a land surface model for the high
908 latitudes: model description and validation, *Geoscientific Model Development*, 11, 121, 2018.

909 Haverd, V., Smith, B., Nieradzki, L., Briggs, P. R., Woodgate, W., Trudinger, C. M., Canadell, J. G.,
910 and Cuntz, M.: A new version of the CABLE land surface model (Subversion revision r4601)
911 incorporating land use and land cover change, woody vegetation demography, and a novel
912 optimisation-based approach to plant coordination of photosynthesis, *Geosci. Model Dev.*, 11,
913 2995-3026, 2018.

914 Heijmans, M. M., Arp, W. J., and Berendse, F.: Effects of elevated CO₂ and vascular plants on
915 evapotranspiration in bog vegetation, *Global Change Biology*, 7, 817-827, 2001.

916 Hu, Z., Shi, H., Cheng, K., Wang, Y. P., Piao, S., Li, Y., Zhang, L., Xia, J., Zhou, L., and Yuan, W.:
917 Joint structural and physiological control on the interannual variation in productivity in a
918 temperate grassland: A data - model comparison, *Global change biology*, 24, 2965-2979, 2018.

919 Huang, S., Bartlett, P., and Arain, M. A.: Assessing nitrogen controls on carbon, water and
920 energy exchanges in major plant functional types across North America using a carbon and
921 nitrogen coupled ecosystem model, *Ecological modelling*, 323, 12-27, 2016.

922 Hulley, G., Hook, S., Fisher, J., and Lee, C.: ECOSTRESS, A NASA Earth-Ventures Instrument for
923 studying links between the water cycle and plant health over the diurnal cycle, 2017 IEEE
924 International Geoscience and Remote Sensing Symposium (IGARSS), 2017, 5494-5496.

925 Ito, A.: Evaluation of the impacts of defoliation by tropical cyclones on a Japanese forest's
926 carbon budget using flux data and a process - based model, *Journal of Geophysical Research:
927 Biogeosciences*, 115, 2010.

928 Jackson, R., Reginato, R., and Idso, S.: Wheat canopy temperature: a practical tool for
929 evaluating water requirements, *Water resources research*, 13, 651-656, 1977.

930 Jimenez, C., Prigent, C., Mueller, B., Seneviratne, S. I., McCabe, M., Wood, E., Rossow, W.,
931 Balsamo, G., Betts, A., and Dirmeyer, P.: Global intercomparison of 12 land surface heat flux
932 estimates, *Journal of Geophysical Research: Atmospheres*, 116, 2011.

933 Jung, M., Koirala, S., Weber, U., Ichii, K., Gans, F., Camps-Valls, G., Papale, D., Schwalm, C.,
934 Tramontana, G., and Reichstein, M.: The FLUXCOM ensemble of global land-atmosphere energy
935 fluxes, *Scientific Data*, 6, 74, 2019.

936 Jung, M., Reichstein, M., and Bondeau, A.: Towards global empirical upscaling of FLUXNET eddy
937 covariance observations: validation of a model tree ensemble approach using a biosphere
938 model, *Biogeosciences*, 6, 2001-2013, 2009.

939 Jung, M., Reichstein, M., Ciais, P., Seneviratne, S. I., Sheffield, J., Goulden, M. L., Bonan, G.,
940 Cescatti, A., Chen, J., and De Jeu, R.: Recent decline in the global land evapotranspiration trend
941 due to limited moisture supply, *Nature*, 467, 951, 2010.

942 Jung, M., Reichstein, M., Margolis, H. A., Cescatti, A., Richardson, A. D., Arain, M. A., Arneth, A.,
943 Bernhofer, C., Bonal, D., and Chen, J.: Global patterns of land - atmosphere fluxes of carbon
944 dioxide, latent heat, and sensible heat derived from eddy covariance, satellite, and
945 meteorological observations, *Journal of Geophysical Research: Biogeosciences*, 116, 2011.

946 Jung, M., Reichstein, M., Schwalm, C. R., Huntingford, C., Sitch, S., Ahlström, A., Arneth, A.,
947 Camps-Valls, G., Ciais, P., and Friedlingstein, P.: Compensatory water effects link yearly global
948 land CO₂ sink changes to temperature, *Nature*, 541, 516-520, 2017.

949 Ke, Y., Im, J., Park, S., and Gong, H.: Downscaling of MODIS One kilometer evapotranspiration
950 using Landsat-8 data and machine learning approaches, *Remote Sensing*, 8, 215, 2016.

951 Keller, K. M., Lienert, S., Bozbiyik, A., Stocker, T. F., Frank, D. C., Klesse, S., Koven, C. D.,
952 Leuenberger, M., Riley, W. J., and Saurer, M.: 20th century changes in carbon isotopes and
953 water-use efficiency: tree-ring-based evaluation of the CLM4. 5 and LPX-Bern models,
954 *Biogeosciences (Online)*, 14, 2017.

955 Kendall, M. G.: Rank correlation methods, 1955. 1955.

956 Khan, M. S., Liaqat, U. W., Baik, J., and Choi, M.: Stand-alone uncertainty characterization of
957 GLEAM, GLDAS and MOD16 evapotranspiration products using an extended triple collocation
958 approach, *Agricultural and Forest Meteorology*, 252, 256-268, 2018.

959 Kisi, O., Sanikhani, H., Zounemat-Kermani, M., and Niazi, F.: Long-term monthly
960 evapotranspiration modeling by several data-driven methods without climatic data, *Computers
961 and Electronics in Agriculture*, 115, 66-77, 2015.

962 Kişi, Ö. and Tombul, M.: Modeling monthly pan evaporations using fuzzy genetic approach,
963 *Journal of hydrology*, 477, 203-212, 2013.

964 Knauer, J., Werner, C., and Zaehle, S.: Evaluating stomatal models and their atmospheric
965 drought response in a land surface scheme: A multibiome analysis, *Journal of Geophysical
966 Research: Biogeosciences*, 120, 1894-1911, 2015.

967 Lawrence, D. M., Thornton, P. E., Oleson, K. W., and Bonan, G. B.: The partitioning of
968 evapotranspiration into transpiration, soil evaporation, and canopy evaporation in a GCM:
969 Impacts on land-atmosphere interaction, *Journal of Hydrometeorology*, 8, 862-880, 2007.

970 Le Quéré, C., Andrew, R. M., Friedlingstein, P., Sitch, S., Pongratz, J., Manning, A. C.,
971 Korsbakken, J. I., Peters, G. P., Canadell, J. G., and Jackson, R. B.: Global carbon budget 2017,
972 *Earth Syst. Sci. Data*, 10, 405-448, 2018.

973 Leipprand, A. and Gerten, D.: Global effects of doubled atmospheric CO₂ content on
974 evapotranspiration, soil moisture and runoff under potential natural vegetation, *Hydrological
975 Sciences Journal*, 51, 171-185, 2006.

976 Leuning, R., Zhang, Y., Rajaud, A., Cleugh, H., and Tu, K.: A simple surface conductance model to
977 estimate regional evaporation using MODIS leaf area index and the Penman - Monteith
978 equation, *Water Resources Research*, 44, 2008.

979 Li, J., Wang, Y. P., Duan, Q., Lu, X., Pak, B., Wiltshire, A., Robertson, E., and Ziehn, T.:
980 Quantification and attribution of errors in the simulated annual gross primary production and
981 latent heat fluxes by two global land surface models, *Journal of Advances in Modeling Earth*
982 *Systems*, 8, 1270-1288, 2016.

983 Li, L., Wang, Y. P., Yu, Q., Pak, B., Eamus, D., Yan, J., Gorsel, E., and Baker, I. T.: Improving the
984 responses of the Australian community land surface model (CABLE) to seasonal drought,
985 *Journal of Geophysical Research: Biogeosciences*, 117, 2012.

986 Li, Z.-L., Tang, R., Wan, Z., Bi, Y., Zhou, C., Tang, B., Yan, G., and Zhang, X.: A review of current
987 methodologies for regional evapotranspiration estimation from remotely sensed data, *Sensors*,
988 9, 3801-3853, 2009.

989 Lian, X., Piao, S., Huntingford, C., Li, Y., Zeng, Z., Wang, X., Ciais, P., McVicar, T. R., Peng, S., and
990 Ottlé, C.: Partitioning global land evapotranspiration using CMIP5 models constrained by
991 observations, *Nature Climate Change*, 8, 640, 2018.

992 Liu, M., Tian, H., Chen, G., Ren, W., Zhang, C., and Liu, J.: Effects of Land - Use and Land - Cover
993 Change on Evapotranspiration and Water Yield in China During 1900 - 2000 1, *JAWRA Journal*
994 *of the American Water Resources Association*, 44, 1193-1207, 2008.

995 Ma, Y., Liu, S., Song, L., Xu, Z., Liu, Y., Xu, T., and Zhu, Z.: Estimation of daily evapotranspiration
996 and irrigation water efficiency at a Landsat-like scale for an arid irrigation area using multi-
997 source remote sensing data, *Remote Sensing of Environment*, 216, 715-734, 2018.

998 Mann, H. B.: Nonparametric tests against trend, *Econometrica: Journal of the Econometric*
999 *Society*, 1945. 245-259, 1945.

1000 Mao, J., Fu, W., Shi, X., Ricciuto, D. M., Fisher, J. B., Dickinson, R. E., Wei, Y., Shem, W., Piao, S.,
1001 and Wang, K.: Disentangling climatic and anthropogenic controls on global terrestrial
1002 evapotranspiration trends, *Environmental Research Letters*, 10, 094008, 2015.

1003 Mao, J., Ribes, A., Yan, B., Shi, X., Thornton, P. E., Séférian, R., Ciais, P., Myneni, R. B., Douville,
1004 H., and Piao, S.: Human-induced greening of the northern extratropical land surface, *Nature*
1005 *Climate Change*, 2016. 2016.

1006 Martens, B., Gonzalez Miralles, D., Lievens, H., van der Schalie, R., de Jeu, R. A., Fernández-
1007 Prieto, D., Beck, H. E., Dorigo, W., and Verhoest, N.: GLEAM v3: Satellite-based land evaporation
1008 and root-zone soil moisture, *Geoscientific Model Development*, 10, 1903-1925, 2017.

1009 Maselli, F., Papale, D., Chiesi, M., Matteucci, G., Angeli, L., Raschi, A., and Seufert, G.:
1010 Operational monitoring of daily evapotranspiration by the combination of MODIS NDVI and
1011 ground meteorological data: Application and evaluation in Central Italy, *Remote sensing of*
1012 *environment*, 152, 279-290, 2014.

1013 Medlyn, B. E., Zaehle, S., De Kauwe, M. G., Walker, A. P., Dietze, M. C., Hanson, P. J., Hickler, T.,
1014 Jain, A. K., Luo, Y., and Parton, W.: Using ecosystem experiments to improve vegetation models,
1015 *Nature Climate Change*, 5, 528, 2015.

1016 Miralles, D., Holmes, T., De Jeu, R., Gash, J., Meesters, A., and Dolman, A.: Global land-surface
1017 evaporation estimated from satellite-based observations, *Hydrology and Earth System Sciences*,
1018 15, 453-469, 2011.

1019 Miralles, D., Jiménez, C., Jung, M., Michel, D., Ershadi, A., McCabe, M., Hirschi, M., Martens, B.,
1020 Dolman, A., and Fisher, J.: The WACMOS-ET project-Part 2: Evaluation of global terrestrial
1021 evaporation data sets, *Hydrology and Earth System Sciences*, 20, 823-842, 2016.

1022 Miralles, D., van den Berg, M., Gash, J., Parinussa, R., Jeu, R., Beck, H., Holmes, T., Jimenez, C.,
1023 Verhoest, N., and Dorigo, W.: El Nino-La Nina cycle and recent trends in continental
1024 evaporation, *Nature Climate Change*, 4, 122-126, 2014.
1025 Monteith, J. L.: Evaporation and environment, 1965, 4.
1026 Mu, Q., Heinsch, F. A., Zhao, M., and Running, S. W.: Development of a global
1027 evapotranspiration algorithm based on MODIS and global meteorology data, *Remote sensing of*
1028 *Environment*, 111, 519-536, 2007.
1029 Mu, Q., Zhao, M., and Running, S. W.: Improvements to a MODIS global terrestrial
1030 evapotranspiration algorithm, *Remote Sensing of Environment*, 115, 1781-1800, 2011.
1031 Mueller, B., Hirschi, M., Jimenez, C., Ciais, P., Dirmeyer, P., Dolman, A., Fisher, J., Jung, M.,
1032 Ludwig, F., and Maignan, F.: Benchmark products for land evapotranspiration: LandFlux-EVAL
1033 multi-data set synthesis, *Hydrology and Earth System Sciences*, 2013. 2013.
1034 Mueller, B., Seneviratne, S. I., Jimenez, C., Corti, T., Hirschi, M., Balsamo, G., Ciais, P., Dirmeyer,
1035 P., Fisher, J., and Guo, Z.: Evaluation of global observations - based evapotranspiration datasets
1036 and IPCC AR4 simulations, *Geophysical Research Letters*, 38, 2011.
1037 Murray-Tortarolo, G., Anav, A., Friedlingstein, P., Sitch, S., Piao, S., Zhu, Z., Poulter, B., Zaehle,
1038 S., Ahlström, A., and Lomas, M.: Evaluation of land surface models in reproducing satellite-
1039 derived LAI over the high-latitude northern hemisphere. Part I: Uncoupled DGVMs, *Remote*
1040 *Sensing*, 5, 4819-4838, 2013.
1041 Nagler, P. L., Scott, R. L., Westenburg, C., Cleverly, J. R., Glenn, E. P., and Huete, A. R.:
1042 Evapotranspiration on western US rivers estimated using the Enhanced Vegetation Index from
1043 MODIS and data from eddy covariance and Bowen ratio flux towers, *Remote sensing of*
1044 *environment*, 97, 337-351, 2005.
1045 Nepstad, D., Lefebvre, P., Lopes da Silva, U., Tomasella, J., Schlesinger, P., Solórzano, L.,
1046 Moutinho, P., Ray, D., and Guerreira Benito, J.: Amazon drought and its implications for forest
1047 flammability and tree growth: A basin - wide analysis, *Global change biology*, 10, 704-717,
1048 2004.
1049 Niu, G. Y., Yang, Z. L., Mitchell, K. E., Chen, F., Ek, M. B., Barlage, M., Kumar, A., Manning, K.,
1050 Niyogi, D., and Rosero, E.: The community Noah land surface model with multiparameterization
1051 options (Noah - MP): 1. Model description and evaluation with local - scale measurements,
1052 *Journal of Geophysical Research: Atmospheres*, 116, 2011.
1053 Noilhan, J. and Mahfouf, J.-F.: The ISBA land surface parameterisation scheme, *Global and*
1054 *planetary Change*, 13, 145-159, 1996.
1055 Norman, J. M. and Becker, F.: Terminology in thermal infrared remote sensing of natural
1056 surfaces, *Remote Sensing Reviews*, 12, 159-173, 1995.
1057 Oki, T. and Kanae, S.: Global hydrological cycles and world water resources, *science*, 313, 1068-
1058 1072, 2006.
1059 Oleson, K. W., Lawrence, D. M., Gordon, B., Flanner, M. G., Kluzek, E., Peter, J., Levis, S.,
1060 Swenson, S. C., Thornton, E., and Feddema, J.: Technical description of version 4.0 of the
1061 Community Land Model (CLM), 2010. 2010.
1062 Pagán, R. B., Maes, H. W., Gentile, P., Martens, B., and Miralles, G. D.: Exploring the Potential
1063 of Satellite Solar-Induced Fluorescence to Constrain Global Transpiration Estimates, *Remote*
1064 *Sensing*, 11, 2019.

1065 Pan, N., Feng, X., Fu, B., Wang, S., Ji, F., and Pan, S.: Increasing global vegetation browning
1066 hidden in overall vegetation greening: Insights from time-varying trends, *Remote Sensing of*
1067 *Environment*, 214, 59-72, 2018a.

1068 Pan, S., Chen, G., Ren, W., Dangal, S. R. S., Banger, K., Yang, J., Tao, B., and Tian, H.: Responses
1069 of global terrestrial water use efficiency to climate change and rising atmospheric CO₂
1070 concentration in the twenty-first century, *International Journal of Digital Earth*, 11, 558-582,
1071 2018b.

1072 Pan, S., Tian, H., Dangal, S. R., Yang, Q., Yang, J., Lu, C., Tao, B., Ren, W., and Ouyang, Z.:
1073 Responses of global terrestrial evapotranspiration to climate change and increasing
1074 atmospheric CO₂ in the 21st century, *Earth's Future*, 3, 15-35, 2015.

1075 Peng, S., Piao, S., Ciais, P., Myneni, R. B., Chen, A., Chevallier, F., Dolman, A. J., Janssens, I. A.,
1076 Penuelas, J., and Zhang, G.: Asymmetric effects of daytime and night-time warming on Northern
1077 Hemisphere vegetation, *Nature*, 501, 88, 2013.

1078 Peterson, T. C., Golubev, V. S., and Groisman, P. Y.: Evaporation losing its strength, *Nature*, 377,
1079 687-688, 1995.

1080 Piao, S., Ciais, P., Huang, Y., Shen, Z., Peng, S., Li, J., Zhou, L., Liu, H., Ma, Y., and Ding, Y.: The
1081 impacts of climate change on water resources and agriculture in China, *Nature*, 467, 43-51,
1082 2010.

1083 Poon, P. and Kinoshita, A.: Estimating Evapotranspiration in a Post-Fire Environment Using
1084 Remote Sensing and Machine Learning, *Remote Sensing*, 10, 1728, 2018.

1085 Priestley, C. and Taylor, R.: On the assessment of surface heat flux and evaporation using large-
1086 scale parameters, *Monthly weather review*, 100, 81-92, 1972.

1087 Purdy, A. J., Fisher, J. B., Goulden, M. L., Colliander, A., Halverson, G., Tu, K., and Famiglietti, J.
1088 S.: SMAP soil moisture improves global evapotranspiration, *Remote Sensing of Environment*,
1089 219, 1-14, 2018.

1090 Reichstein, M., Besnard, S., Carvalhais, N., Gans, F., Jung, M., Kraft, B., and Mahecha, M.:
1091 Modelling Landsurface Time-Series with Recurrent Neural Nets, *IGARSS 2018-2018 IEEE*
1092 *International Geoscience and Remote Sensing Symposium*2018, 7640-7643.

1093 Reichstein, M., Camps-Valls, G., Stevens, B., Jung, M., Denzler, J., Carvalhais, N., and Prabhat:
1094 Deep learning and process understanding for data-driven Earth system science, *Nature*, 566,
1095 195-204, 2019.

1096 Restrepo - Coupe, N., Levine, N. M., Christoffersen, B. O., Albert, L. P., Wu, J., Costa, M. H.,
1097 Galbraith, D., Imbuzeiro, H., Martins, G., and da Araujo, A. C.: Do dynamic global vegetation
1098 models capture the seasonality of carbon fluxes in the Amazon basin? A data - model
1099 intercomparison, *Global change biology*, 23, 191-208, 2017.

1100 Roderick, M. L. and Farquhar, G. D.: The cause of decreased pan evaporation over the past 50
1101 years, *science*, 298, 1410-1411, 2002.

1102 Rouholahnejad, E. and Martens, B.: Improving global estimates of terrestrial evaporation by
1103 integrating remotely-sensed observations of changes in terrestrial water storage (GRACE) into a
1104 global evaporation model (GLEAM), 2018 2018.

1105 Running, S. W.: A measurable planetary boundary for the biosphere, *science*, 337, 1458-1459,
1106 2012.

1107 Sayemuzzaman, M. and Jha, M. K.: Seasonal and annual precipitation time series trend analysis
1108 in North Carolina, United States, *Atmospheric Research*, 137, 183-194, 2014.

1109 Semmens, K. A., Anderson, M. C., Kustas, W. P., Gao, F., Alfieri, J. G., McKee, L., Prueger, J. H.,
 1110 Hain, C. R., Cammalleri, C., Yang, Y., Xia, T., Sanchez, L., Mar Alsina, M., and Vélez, M.:
 1111 Monitoring daily evapotranspiration over two California vineyards using Landsat 8 in a multi-
 1112 sensor data fusion approach, *Remote Sensing of Environment*, 185, 155-170, 2016.
 1113 Sen, P. K.: Estimates of the regression coefficient based on Kendall's tau, *Journal of the*
 1114 *American statistical association*, 63, 1379-1389, 1968.
 1115 Shrestha, N. and Shukla, S.: Support vector machine based modeling of evapotranspiration
 1116 using hydro-climatic variables in a sub-tropical environment, *Agricultural and forest*
 1117 *meteorology*, 200, 172-184, 2015.
 1118 Siebert, S., Burke, J., Faures, J.-M., Frenken, K., Hoogeveen, J., Döll, P., and Portmann, F. T.:
 1119 Groundwater use for irrigation—a global inventory, *Hydrology and earth system sciences*, 14,
 1120 1863-1880, 2010.
 1121 Simmons, A., Willett, K., Jones, P., Thorne, P., and Dee, D.: Low - frequency variations in surface
 1122 atmospheric humidity, temperature, and precipitation: Inferences from reanalyses and monthly
 1123 gridded observational data sets, *Journal of Geophysical Research: Atmospheres*, 115, 2010.
 1124 Sitch, S., Smith, B., Prentice, I. C., Arneth, A., Bondeau, A., Cramer, W., Kaplan, J., Levis, S.,
 1125 Lucht, W., and Sykes, M. T.: Evaluation of ecosystem dynamics, plant geography and terrestrial
 1126 carbon cycling in the LPJ dynamic global vegetation model, *Global Change Biology*, 9, 161-185,
 1127 2003.
 1128 Smith, B.: LPJ-GUESS-an ecosystem modelling framework, *Department of Physical Geography*
 1129 *and Ecosystems Analysis. INES, Sölvegatan*, 12, 22362, 2001.
 1130 Steffen, W., Richardson, K., Rockström, J., Cornell, S. E., Fetzer, I., Bennett, E. M., Biggs, R.,
 1131 Carpenter, S. R., de Vries, W., de Wit, C. A., Folke, C., Gerten, D., Heinke, J., Mace, G. M.,
 1132 Persson, L. M., Ramanathan, V., Reyers, B., and Sörlin, S.: Planetary boundaries: Guiding human
 1133 development on a changing planet, *Science*, 347, 1259855, 2015.
 1134 Stoy, P. C., El-Madany, T., Fisher, J. B., Gentile, P., Gerken, T., Good, S. P., Liu, S., Miralles, D. G.,
 1135 Perez-Priego, O., Skaggs, T. H., Wohlfahrt, G., Anderson, R. G., Jung, M., Maes, W. H.,
 1136 Mammarella, I., Mauder, M., Migliavacca, M., Nelson, J. A., Poyatos, R., Reichstein, M., Scott, R.
 1137 L., and Wolf, S.: Reviews and syntheses: Turning the challenges of partitioning ecosystem
 1138 evaporation and transpiration into opportunities, *Biogeosciences Discuss.*, 2019, 1-47, 2019.
 1139 Sun, Q., Miao, C., Duan, Q., Ashouri, H., Sorooshian, S., and Hsu, K. L.: A review of global
 1140 precipitation data sets: Data sources, estimation, and intercomparisons, *Reviews of Geophysics*,
 1141 56, 79-107, 2018.
 1142 Sun, Y., Frankenberg, C., Wood, J. D., Schimel, D. S., Jung, M., Guanter, L., Drewry, D. T., Verma,
 1143 M., Porcar-Castell, A., Griffis, T. J., Gu, L., Magney, T. S., Köhler, P., Evans, B., and Yuen, K.: OCO-
 1144 2 advances photosynthesis observation from space via solar-induced chlorophyll fluorescence,
 1145 *Science*, 358, eaam5747, 2017.
 1146 Swann, A. L., Hoffman, F. M., Koven, C. D., and Randerson, J. T.: Plant responses to increasing
 1147 CO2 reduce estimates of climate impacts on drought severity, *Proceedings of the National*
 1148 *Academy of Sciences*, 113, 10019-10024, 2016.
 1149 Szutu, D. J. and Papuga, S. A.: Year-Round Transpiration Dynamics Linked With Deep Soil
 1150 Moisture in a Warm Desert Shrubland, *Water Resources Research*, 0, 2019.

1151 Tabari, H., Martinez, C., Ezani, A., and Talaei, P. H.: Applicability of support vector machines
1152 and adaptive neurofuzzy inference system for modeling potato crop evapotranspiration,
1153 Irrigation science, 31, 575-588, 2013.

1154 Talsma, C., Good, S., Miralles, D., Fisher, J., Martens, B., Jimenez, C., and Purdy, A.: Sensitivity of
1155 Evapotranspiration Components in Remote Sensing-Based Models, Remote Sensing, 10, 1601,
1156 2018a.

1157 Talsma, C. J., Good, S. P., Jimenez, C., Martens, B., Fisher, J. B., Miralles, D. G., McCabe, M. F.,
1158 and Purdy, A. J.: Partitioning of evapotranspiration in remote sensing-based models,
1159 Agricultural and Forest Meteorology, 260-261, 131-143, 2018b.

1160 Tian, H., Chen, G., Liu, M., Zhang, C., Sun, G., Lu, C., Xu, X., Ren, W., Pan, S., and Chappelka, A.:
1161 Model estimates of net primary productivity, evapotranspiration, and water use efficiency in
1162 the terrestrial ecosystems of the southern United States during 1895–2007, Forest ecology and
1163 management, 259, 1311-1327, 2010.

1164 Trenberth, K. E., Fasullo, J. T., and Kiehl, J.: Earth's global energy budget, Bulletin of the
1165 American Meteorological Society, 90, 311-324, 2009.

1166 Vinukollu, R. K., Meynadier, R., Sheffield, J., and Wood, E. F.: Multi - model, multi - sensor
1167 estimates of global evapotranspiration: Climatology, uncertainties and trends, Hydrological
1168 Processes, 25, 3993-4010, 2011a.

1169 Vinukollu, R. K., Wood, E. F., Ferguson, C. R., and Fisher, J. B.: Global estimates of
1170 evapotranspiration for climate studies using multi-sensor remote sensing data: Evaluation of
1171 three process-based approaches, Remote Sensing of Environment, 115, 801-823, 2011b.

1172 Wang, K. and Dickinson, R. E.: A review of global terrestrial evapotranspiration: Observation,
1173 modeling, climatology, and climatic variability, Reviews of Geophysics, 50, 2012.

1174 Wang, K., Dickinson, R. E., Wild, M., and Liang, S.: Evidence for decadal variation in global
1175 terrestrial evapotranspiration between 1982 and 2002: 1. Model development, Journal of
1176 Geophysical Research: Atmospheres, 115, D20112, 2010.

1177 Wartenburger, R., Seneviratne, S. I., Hirschi, M., Chang, J., Ciais, P., Deryng, D., Elliott, J.,
1178 Folberth, C., Gosling, S. N., and Gudmundsson, L.: Evapotranspiration simulations in ISIMIP2a-
1179 Evaluation of spatio-temporal characteristics with a comprehensive ensemble of independent
1180 datasets, Environmental Research Letters, 13, 075001, 2018.

1181 Willett, K. M., Gillett, N. P., Jones, P. D., and Thorne, P. W.: Attribution of observed surface
1182 humidity changes to human influence, Nature, 449, 710, 2007.

1183 Xu, D., Agee, E., Wang, J., and Ivanov, V. Y.: Estimation of Evapotranspiration of Amazon
1184 Rainforest Using the Maximum Entropy Production Method, Geophysical Research Letters, 0,
1185 2019.

1186 Xu, T., Guo, Z., Liu, S., He, X., Meng, Y., Xu, Z., Xia, Y., Xiao, J., Zhang, Y., Ma, Y., and Song, L.:
1187 Evaluating Different Machine Learning Methods for Upscaling Evapotranspiration from Flux
1188 Towers to the Regional Scale, Journal of Geophysical Research: Atmospheres, 123, 8674-8690,
1189 2018.

1190 Yao, Y., Liang, S., Cheng, J., Liu, S., Fisher, J. B., Zhang, X., Jia, K., Zhao, X., Qin, Q., and Zhao, B.:
1191 MODIS-driven estimation of terrestrial latent heat flux in China based on a modified Priestley–
1192 Taylor algorithm, Agricultural and Forest Meteorology, 171, 187-202, 2013.

1193 Yao, Y., Liang, S., Li, X., Chen, J., Liu, S., Jia, K., Zhang, X., Xiao, Z., Fisher, J. B., and Mu, Q.:
1194 Improving global terrestrial evapotranspiration estimation using support vector machine by

1195 integrating three process-based algorithms, *Agricultural and forest meteorology*, 242, 55-74,
1196 2017.

1197 Yao, Y., Liang, S., Li, X., Liu, S., Chen, J., Zhang, X., Jia, K., Jiang, B., Xie, X., and Munier, S.:
1198 Assessment and simulation of global terrestrial latent heat flux by synthesis of CMIP5 climate
1199 models and surface eddy covariance observations, *Agricultural and forest meteorology*, 223,
1200 151-167, 2016.

1201 Yuan, W., Liu, S., Liu, H., Randerson, J. T., Yu, G., and Tieszen, L. L.: Impacts of precipitation
1202 seasonality and ecosystem types on evapotranspiration in the Yukon River Basin, Alaska, *Water
1203 Resources Research*, 46, 2010.

1204 Yue, S., Pilon, P., and Cavadias, G.: Power of the Mann–Kendall and Spearman's rho tests for
1205 detecting monotonic trends in hydrological series, *Journal of hydrology*, 259, 254-271, 2002.

1206 Zaehle, S. and Friend, A.: Carbon and nitrogen cycle dynamics in the O - CN land surface model:
1207 1. Model description, site - scale evaluation, and sensitivity to parameter estimates, *Global
1208 Biogeochemical Cycles*, 24, 2010.

1209 Zeng, Z., Peng, L., and Piao, S.: Response of terrestrial evapotranspiration to Earth's greening,
1210 *Current Opinion in Environmental Sustainability*, 33, 9-25, 2018a.

1211 Zeng, Z., Piao, S., Li, L. Z., Wang, T., Ciais, P., Lian, X., Yang, Y., Mao, J., Shi, X., and Myneni, R. B.:
1212 Impact of Earth greening on the terrestrial water cycle, *Journal of Climate*, 31, 2633-2650,
1213 2018b.

1214 Zeng, Z., Piao, S., Lin, X., Yin, G., Peng, S., Ciais, P., and Myneni, R. B.: Global evapotranspiration
1215 over the past three decades: estimation based on the water balance equation combined with
1216 empirical models, *Environmental Research Letters*, 7, 014026, 2012.

1217 Zeng, Z., Wang, T., Zhou, F., Ciais, P., Mao, J., Shi, X., and Piao, S.: A worldwide analysis of
1218 spatiotemporal changes in water balance - based evapotranspiration from 1982 to 2009,
1219 *Journal of Geophysical Research: Atmospheres*, 119, 1186-1202, 2014.

1220 Zeng, Z., Zhu, Z., Lian, X., Li, L. Z., Chen, A., He, X., and Piao, S.: Responses of land
1221 evapotranspiration to Earth's greening in CMIP5 Earth System Models, *Environmental Research
1222 Letters*, 11, 104006, 2016.

1223 Zhang, K., Kimball, J. S., Nemani, R. R., and Running, S. W.: A continuous satellite - derived
1224 global record of land surface evapotranspiration from 1983 to 2006, *Water Resources Research*,
1225 46, 2010.

1226 Zhang, K., Kimball, J. S., Nemani, R. R., Running, S. W., Hong, Y., Gourley, J. J., and Yu, Z.:
1227 Vegetation greening and climate change promote multidecadal rises of global land
1228 evapotranspiration, *Scientific reports*, 5, 15956, 2015.

1229 Zhang, K., Kimball, J. S., and Running, S. W.: A review of remote sensing based actual
1230 evapotranspiration estimation, *Wiley Interdisciplinary Reviews: Water*, 3, 834-853, 2016a.

1231 Zhang, L., Lei, H., Shen, H., Cong, Z., Yang, D., and Liu, T.: Evaluating the Representation of
1232 Vegetation Phenology in the Community Land Model 4.5 in a Temperate Grassland, *Journal of
1233 Geophysical Research: Biogeosciences*, 124, 187-210, 2019.

1234 Zhang, Y., Peña-Arancibia, J. L., McVicar, T. R., Chiew, F. H., Vaze, J., Liu, C., Lu, X., Zheng, H.,
1235 Wang, Y., and Liu, Y. Y.: Multi-decadal trends in global terrestrial evapotranspiration and its
1236 components, *Scientific reports*, 6, 19124, 2016b.

1237 Zhu, Z., Bi, J., Pan, Y., Ganguly, S., Anav, A., Xu, L., Samanta, A., Piao, S., Nemani, R. R., and
1238 Myneni, R. B.: Global data sets of vegetation leaf area index (LAI) 3g and Fraction of
1239 Photosynthetically Active Radiation (FPAR) 3g derived from Global Inventory Modeling and
1240 Mapping Studies (GIMMS) Normalized Difference Vegetation Index (NDVI3g) for the period
1241 1981 to 2011, *Remote Sensing*, 5, 927-948, 2013.
1242 Zhu, Z., Piao, S., Myneni, R. B., Huang, M., Zeng, Z., Canadell, J. G., Ciais, P., Sitch, S.,
1243 Friedlingstein, P., and Arneeth, A.: Greening of the Earth and its drivers, *Nature Climate Change*,
1244 2016. 2016.

1245 **Table 1.** Descriptions of models used in this study, including their drivers, adopted algorithms,
 1246 key equations, limitations and references

Name	Input	Algorithm	Spatial resolution	Temporal resolution	Key equations	Limitations	References
MTE	Climate: precipitation, temperature, sunshine hour, relative humidity, wet days Vegetation: fAPAR	TRIAL ERROR	+0.5°×0.5°	Monthly	No specific equation	Insufficient observations in tropical regions; with no CO2 effect	flux Jung et al. (2011)
RF	enhanced vegetation index, fAPAR, leaf area index, land surface temperature, radiation, potential radiation, index of water availability, relative humidity	Randomized decision tree	0.5°×0.5°	Half-hourly	No specific equation	The same with MTE	Bodesheim et al. (2018)
P-LSH	Climate: radiation, temperature, vapor pressure, wind speed, CO2 Vegetation: AVHRR NDVI	Modified air Penman–Monteith	0.083°×0.083°	Monthly	$E_v = \frac{\Delta R_n + \rho C_p VPD g_a}{\lambda_v (\Delta + \gamma \left(1 + \frac{g_a}{g_s}\right))}$ $E_s = RH \frac{VPD}{k} \frac{\Delta R_n + \rho C_p VPD g_a}{\lambda_v (\Delta + \gamma \left(1 + \frac{g_a}{g_s}\right))}$	Advantages: more robust physical basis; consider the effects of CO2 Limitations: high meteorological forcing requirements; canopy conductance is based on proxies;	Zhang et al. (2015)
GLEAM	Climate: precipitation, net radiation, soil moisture, land surface temperature, air temperature, snow depth Vegetation: vegetation optical depth	Modified Priestley–Taylor	0.25°×0.25°	Daily	$E_s = f_s S_s \alpha_s \frac{\Delta}{\lambda_v \rho_w (\Delta + \gamma)} (R_n^s - G_s)$ $E_{sc} = f_{sc} S_{sc} \alpha_{sc} \frac{\Delta}{\lambda_v \rho_w (\Delta + \gamma)} (R_n^{sc} - G_{sc})$ $E_{tc} = f_{tc} S_{tc} \alpha_{tc} \frac{\Delta}{\lambda_v \rho_w (\Delta + \gamma)} (R_n^{tc} - G_{tc}) - \beta E_i$	Advantages: simple; low requirement for meteorological data; well-suited for remote sensing observable variables; soil moisture is considered Limitations: many simplifications of physical processes; neither VPD nor surface and aerodynamic resistances are explicitly accounted for; strong dependency on net radiation	(Miralles et al., 2011)
MODIS	Climate: temperature, shortwave radiation, wind speed, relative humidity, air pressure	air Penman–Leuning	0.05°×0.05°	Monthly	$E_i = f_{wet} f_c \frac{\Delta (R_n - G) + \rho c_p \frac{VPD}{T_a^{wc}}}{\lambda_v \rho_w (\Delta + \gamma \frac{T_a^{wc}}{T_a^c})}$ $E_v = (1 - f_{wet}) f_c \frac{\Delta (R_n - G) + \rho c_p \frac{VPD}{T_a^c}}{\lambda_v \rho_w (\Delta + \gamma \frac{T_a^c}{T_a^i})}$	Advantages: more robust physical basis; Limitations: require many variables that are difficult to observe or not observable with	Mu et al. (2011)

Vegetation:
LAI, fAPAR,
albedo

$$E_s = [f_{wet} + \frac{(1-f_{wet})hVPD}{\beta}] \left(sA_{soil} + \frac{\rho c_p (1-f_c)VPD}{\lambda_v \rho_w (S + \gamma \frac{r_{tot}}{r_{as}})} \right)$$

satellites; canopy conductance is based on proxies; do not consider soil moisture but use atmospheric humidity as a surrogate; do not consider the effects of CO₂

PML-CSIRO Climate: Penman-Monteith-Leuning
precipitation, air temperature, vapor pressure, shortwave radiation, longwave radiation, wind speed
Vegetation: AVHRR LAI, emissivity and albedo

$$E_v = \frac{\Delta R_n + \rho c_p VPD g_a}{\lambda_v (\Delta + \gamma \left(1 + \frac{g_a}{g_s} \right))}$$

$$E_s = \frac{f \Delta A_s}{\Delta + \gamma}$$

E_v: an adapted version of Gash rainfall interception model (Van et al., 2001)

Advantages: Zhang et al. (2016b) more robust physical basis (compared to Priestley-Taylor equation);

biophysically based estimation of surface conductance

Limitations: high meteorological forcing requirements; canopy conductance is based on proxies; do not consider the effects of CO₂

TRENDY LSMs

Advantages: land surface models are process-oriented and physically-based. Given their structure almost all models are capable to allow factorial analysis, where one forcing can be applied at a time. Most models also consider the physiological effect of CO₂ on stomatal closure.

Formatted: Subscript

Disadvantages: most models typically do not allow integration/assimilation of observation-based vegetation characteristics. Model parameterizations remain uncertain and a same process is modelled in different ways across models. Model parameters may or may not be physically-based and therefore measurable in the field.

Models participating in the TRENDY_{v6-2017} comparison were forced by precipitation, air temperature, specific humidity, shortwave radiation, longwave radiation, wind speed based on the CRU-NCEPv8 data as explained in Le Quere et al. 2018. It is very difficult to list all key equations for all land surface models. Here, we just list the stomatal conductance equation for each model.

Name	Algorithm	Spatial resolution	Temporal resolution	Key equations	References
CABLE	Penman-Monteith	0.5°×0.5°	Monthly	$g_s = g_0 + \frac{g_1 f_w A}{c_a - c_p} \left(1 + \frac{VPD}{VPD_0} \right)^{-1}$	Haverd et al. (2018)
CLASS-CTEM	Modified Penman-Monteith	2.8125°×2.8125°	Monthly	$g_c = m \frac{A_n p}{(c_s - \Gamma) (1 + VPD/VPD_0)} + b LAI$	Melton and Arora (2016)
CLM45	Modified Penman-Monteith	1.875°×2.5°	Monthly	$g_s = g_0 + \frac{g_1 A}{c_a} RH$	Oleson et al. (2010)
DLEM	Penman-Monteith	0.5°×0.5°	Monthly	$g_s = \max(g_{smax} r_{corr} b f(ppdf) f(T_{min}) f(VPD) f(CO_2), g_{smin})$	Pan et al. (2015)
ISAM	Modified Penman-Monteith	0.5°×0.5°	Monthly	$g_s = m \frac{A}{C_s / p_{atm}} \times \frac{e_s}{e_t} + b_t \beta_t$	Barman et al. (2014)
JSBACH	Penman-Monteith	3.9131.9 3.9131.9°	Monthly	$g_s = \beta_w \frac{1.6 A_{n,pot}}{c_a - c_{1,pot}}$	Knauer et al. (2015)
JULES	Penman-Monteith	2.5°×3.75°	Monthly	Bare soil conductance: $g_{soil} = \frac{1}{100} \left(\frac{\theta_s}{\theta_c} \right)^2$ Stomatal conductance is calculated by solving the two equations: $A_i = g_s (C_s - C_i) / 1.6;$ $\frac{C_i - \Gamma^*}{C_c - \Gamma^*} = f_0 \left(1 - \frac{\Delta}{q_c} \right)$	Li et al. (2016)
LPJ-GUESS	Equations proposed by Monteith (1995)	0.5°×0.5°	Monthly	$g_s = g_{smin} + \frac{1.6 A_{dt}}{c_a (1 - \lambda_c)}$	Smith (2001)
LPJ-wsl	Priestley-Taylor	0.5°×0.5°	Monthly	$g_s = g_{smin} + \frac{1.6 A_{dt}}{c_a (1 - \lambda_c)}$	Sitch et al. (2003)
LPX-Bern	Modified equation of Monteith (1995)	1°×1°	Monthly	$g_s = g_{smin} + \frac{1.6 A_{dt}}{c_a (1 - \lambda_c)}$	Keller et al. (2017)

O-CN	Modified Penman-Monteith	1°×1°	Monthly	$g_s = g_{smin} + \frac{1.6A_{dt}}{c_a(1-\lambda_c)}$	Zaehle and Friend (2010)
ORCHID EE	Modified Penman-Monteith	0.5°×0.5°	Monthly	$g_s = g_0 + \frac{A + R_d}{c_a - c_p} f_{vpd}$ $g_{soil} = \exp(8.206 - 4.255W/W_{sat})$	d'Orgeval et al. (2008)
ORCHID EE-MICT	Modified Penman-Monteith	0.5°×0.5°	Monthly	$g_s = g_0 + \frac{A + R_d}{c_a - c_p} f_{vpd}$	Guimberteau et al. (2018)
VISIT	Penman-Monteith	0.5°×0.5°	Monthly	$g_s = g_0 + \frac{g_1 f_w A}{c_a - c_p} \left(1 + \frac{VPD}{VPD_0}\right)^{-1}$	Ito (2010)

1247 Notes: A: net assimilation rate; A_{dt}: total daytime net photosynthesis; A_{n,pot}: unstressed net
1248 assimilation rate; b: soil moisture factor; b_l: stomatal conductance intercept; c_a: atmospheric CO₂
1249 concentration; c_c: critical CO₂ concentration; c_i: internal leaf concentration of CO₂; c_{i,pot}: internal
1250 leaf concentration of CO₂ for unstressed conditions; c_s: leaf surface CO₂ concentration; c_p: CO₂
1251 compensation point; e_s: vapor pressure at leaf surface; e_i: saturation vapor pressure inside the leaf;
1252 E_s: soil evaporation; E_c: canopy evapotranspiration; E_{dry}: dry canopy evapotranspiration; E_{wet}: wet
1253 canopy evapotranspiration; E_v: canopy transpiration; E_i: canopy interception; E_{tc}: transpiration
1254 from tall canopy; E_{sc}: transpiration from short canopy; f: fraction of P to equilibrium soil
1255 evaporation; f_s: soil fraction; f_{sc}: short canopy fraction; f_{tc}: tall canopy fraction; f_{vpd}: factor of the
1256 effect of leaf-to-air vapor pressure difference; f_w: a function describing the soil water stress on
1257 stomatal conductance; f_{wet}: relative surface wetness parameter; f₀: the maximum ratio of internal
1258 to external CO₂; f(ppdf): limiting factor of photosynthetic photo flux density; f(T_{min}): limiting factor
1259 of daily minimum temperature; f(VPD): limiting factor of vapor pressure deficit; f(CO₂): limiting
1260 factor of carbon dioxide; G: ground energy flux; g_a: aerodynamic conductance; g_m:
1261 empirical parameter; g_s: stomatal conductance; g_{smax}: maximum stomatal conductance; g_{smin}:
1262 minimum stomatal conductance; g_{soil}: bare soil conductance; g₀: residual stomatal conductance
1263 when the net assimilation rate is 0; g₁: sensitivity of stomatal conductance to assimilation, ambient
1264 CO₂ concentration and environmental controls; I: tall canopy interception loss; m: stomatal
1265 conductance slope; P_{atm}: atmospheric pressure; PE_s: potential soil evaporation; PE_{canopy}: potential
1266 canopy evaporation; q_a: specific air humidity; q_c: critical humidity deficit; q_s: specific humidity of
1267 saturated air; r_a: aerodynamic resistance; r_s: stomatal resistance; R_n: net radiation; R_d: day
1268 respiration; RH: relative humidity; T_s: actual surface temperature; VPD: vapor pressure deficit;
1269 VPD₀: the sensitivity of stomatal conductance to VPD; W: top soil moisture; W_{canopy}: canopy water;
1270 W_{sat}: soil porosity; α: Priestley-Taylor coefficient; α_m: empirical parameter; β: a constant
1271 accounting for the times in which vegetation is wet; β_l: soil water availability factor between 0 and
1272 1; β_w: ~~A scaling factor to account for water stress empirical water stress factor which is a linear~~
1273 ~~function of soil water content~~; β_s: moisture availability function; ρ: air density; γ: psychrometric
1274 constant; λ_v: latent heat of vaporization; λ_c: ratio of intercellular to ambient partial pressure of CO₂;
1275 r_{corr}: correction factor of temperature and air pressure on conductance; Γ*: CO₂ compensation point
1276 when leaf day respiration is zero; θ₁: parameter of moisture concentration in the top soil layer; θ_c:
1277 parameter of moisture concentration in the spatially varying critical soil moisture; Δ: slope of the
1278 vapor pressure curve.

Formatted: Font: 12 pt

1279 **Table 2.** Inter-annual variability (IAV, denoted as standard deviation) and trend of global
 1280 terrestrial ET during 1982-2011 and the contribution of vegetation greening to ET trend. * suggests
 1281 significance of the trend at the 95% confidence level ($p < 0.05$).

	Model	ET IAV (mm yr ⁻¹)	ET Trend (mm yr ⁻²)	Greening-induced ET change (mm yr ⁻²)	Sensitivity of ET to LAI trend (10 ⁻³ m ² m ² m ⁻² per m ² yr ⁻¹)	
Machine learning	MTE	5.93	0.38*	0.09	35.86	2.51*
	P-LSH	9.95	1.07*	0.34	135.46	2.51*
RS models	GLEAM	8.47	0.33*	0.14	55.78	2.51*
	PML-CSIRO	7.18	0.41*	0.36	143.43	2.51*
	RS model mean	7.98	0.62*	0.28	111.55	2.51*
	CABLE	9.63	0.07	0.35	102.64	3.41*
	CLASS-CTEM	12.22	0.35*	0.53	134.52	3.94*
	CLM45	8.68	0.38*	0.31	67.54	4.59*
	DLEM	7.21	0.26*	0.53	200.76	2.64*
	ISAM	7.50	0.22	0.16	32.26	4.96*
	JSBACH	10.12	-0.05	0.50	217.39	2.30*
	JULES	11.33	-0.02	0.34	85.21	3.99*
LSMs	LPJ-GUESS	7.48	0.50*	0.28	160.92	1.74*
	LPJ-wsl	4.77	0.24*	0.19	31.56	6.02*
	LXP-Bern	4.80	0.20*	0.04	4.04	9.90*
	O-CN	10.41	0.32*	0.53	89.23	5.94*
	ORCHIDEE	9.28	-0.17	0.21	96.33	2.18*
	ORCHIDEE-MICT	10.70	-0.34*	0.50	171.23	2.92*
	VISIT	6.31	0.87*	0.70	51.40	13.62*
	LSM mean	7.73	0.23	0.37	79.91	4.63*

Formatted Table

Formatted: Superscript

Formatted: Font: (Asian) PMingLiU, (Asian) Chinese (Taiwan)

1282